

2D Prony–Huang Transform: A New Tool for 2D Spectral Analysis

Jérémie Schmitt, *Member, IEEE*, Nelly Pustelnik, *Member, IEEE*, Pierre Borgnat, *Member, IEEE*,
Patrick Flandrin, *Fellow, IEEE*, and Laurent Condat, *Member, IEEE*

Abstract—This paper provides an extension of the 1D Hilbert–Huang transform for the analysis of images using recent optimization techniques. The proposed method consists of: 1) adaptively decomposing an image into oscillating parts called intrinsic mode functions (IMFs) using a mode decomposition procedure and 2) providing a local spectral analysis of the obtained IMFs in order to get the local amplitudes, frequencies, and orientations. For the decomposition step, we propose two robust 2D mode decompositions based on nonsmooth convex optimization: 1) a genuine 2D approach, which constrains the local extrema of the IMFs and 2) a pseudo-2D approach, which separately constrains the extrema of lines, columns, and diagonals. The spectral analysis step is an optimization strategy based on Prony annihilation property and applied on small square patches of the IMFs. The resulting 2D Prony–Huang transform is validated on simulated and real data.

Index Terms—Empirical mode decomposition, spectral analysis, convex optimization, nonstationary image analysis.

I. INTRODUCTION

AN IMPORTANT challenge in image processing is the retrieval of the local frequencies, amplitudes, and orientations of a nonstationary image. This subject presents several interesting applications for, e.g., texture classification [1], [2], fingerprint analysis [3], [4], ocean wave characterization [5], [6]. To be specific, most of these images can be expressed as a sum of a trend and one (or several) *amplitude modulation - frequency modulation* (AM–FM) component(s). It results that usual spectral analysis techniques (designed for analyzing one AM–FM component [7]) lead to poor performance when such a class of nonstationary images have to be analyzed. In the context of 1D analysis, an efficient strategy known as 1D–Hilbert Huang Transform (HHT) has been proposed in [7]. The goal of this paper is to propose the counterpart of the 1D–HHT for image analysis.

Manuscript received March 27, 2014; revised August 6, 2014; accepted October 4, 2014. Date of publication October 14, 2014; date of current version October 31, 2014. This work was supported by the Agence Nationale de la Recherche under Grant ANR-13-BS03-0002-01. The associate editor coordinating the review of this manuscript and approving it for publication was Prof. David Frakes.

J. Schmitt, N. Pustelnik, P. Borgnat, and P. Flandrin are with the Laboratoire de Physique, Centre National de la Recherche Scientifique, Ecole Normale Supérieure de Lyon, Lyon 69007, France, and also with the Université de Lyon, Lyon 69007, France (e-mail: jeremy.schmitt@ens-lyon.fr; nelly.pustelnik@ens-lyon.fr; pierre.borgnat@ens-lyon.fr; patrick.flandrin@ens-lyon.fr).

L. Condat is with the GIPSA-Laboratory, Centre National de la Recherche Scientifique, University of Grenoble-Alpes, Grenoble 38008, France (e-mail: laurent.condat@gipsa-lab.grenoble-inp.fr).

Color versions of one or more of the figures in this paper are available online at <http://ieeexplore.ieee.org>.

Digital Object Identifier 10.1109/TIP.2014.2363000

The 1D–HHT is an empirical method for analysis AM–FM signals and it favors adaptivity. The objective of 1D–HHT is to extract the instantaneous amplitudes and frequencies from a signal built as a sum of a trend and *intrinsic mode functions* (IMFs). We recall that an IMF is loosely defined as a function oscillating around zero and having symmetric oscillations. To achieve this goal, the 1D–HHT consists in a two-step procedure:

- a **decomposition** step, whose objective is to extract the IMFs from the data,
- **spectral analysis** of each extracted IMF in order to estimate the instantaneous amplitudes and frequencies of each component.

Regarding the first step, an efficient decomposition procedure known as *empirical mode decomposition* (EMD) has been proposed in [7]. It aims at sequentially extracting the IMF through a sifting process that is based on maxima (resp. minima) cubic spline interpolation. The second step aims at computing the analytic signal of each extracted IMF in order to access the instantaneous amplitude and phase (that leads to frequency) of each IMF. Consequently, the 2D counterpart of the 1D–HHT principle requires (i) a bi-dimensional mode decomposition step providing the 2D–IMFs and (ii) a 2D spectral analysis step allowing to extract the instantaneous amplitude, frequency, and orientation of each bi-dimensional IMF.

A generalization of the 1D–HHT for arbitrary space dimensions has already been proposed in [8]. This method combines a multidimensional extension of an EMD based on the computation of local means [9] and a multidimensional generalization of analytic signal defined with the Riesz transform that is called monogenic signal [10], [11]. However, this method, as well as the other EMD based on a sifting procedure and interpolation steps, lacks of robustness as will be discussed further. Another 2D spectral analysis method whose goal is close to a 2D–HHT is the Riesz–Laplace transform proposed by Unser et al. [12]. It combines a 2D wavelet transform with a monogenic analysis [10], [11]. The counterpart of using a wavelet framework is the lack of adaptivity and consequently this method is less suited than EMD for analyzing nonstationary signals such as AM–FM signals. Moreover, both methods use a monogenic analysis in 2D [12] or n-D [8] for the spectral estimation step, which proved to be efficient for amplitude, phase, and orientation estimation but not so efficient for frequency estimation as it will be seen in Section IV.

The aim of this paper is to revisit each of both steps using recent optimization techniques in order to highlight

the importance of the combination of efficient methods for decomposition and for spectral analysis.

The first contribution of this paper concerns a new robust 2D mode decomposition procedure based on convex optimization. Indeed, the existing 2D-EMD methods are based on the sifting procedure whose main drawback is the lack of a rigorous mathematical definition, and consequently of convergence properties [13]–[19], while efficient 1D mode decomposition procedures based on convex optimization have been recently proposed in order to get stronger mathematical guarantees [20]–[22]. For instance, [22] proposed a mathematical formalism for 1D-EMD based on a multicomponent proximal algorithm that combines the principle of texture-geometry decomposition [23]–[25] with some specific features of the usual EMD: constraints on extrema in order to extract IMFs oscillating around zero, sequential formulation of the usual EMD, or IMFs quasi-orthogonality. This method appears to have better performance (in terms of extraction or convergence guarantees) than the other convex optimization procedures as discussed in [22]. For this reason, we propose to extend this method to a 2D mode decomposition formalism.

Our second contribution concerns an alternative approach to monogenic analysis, based on *annihilation* property [26]–[29]. This property, which was highlighted in Prony work in the eighteenth century [27], is particularly interesting for estimating sinusoids. This annihilation technique has been adapted to the finite rate of innovation problems in [30]. When noise is involved in the data, the procedure is modified in order to incorporate a low rank constraint. This method is known as the Cadzow algorithm [30], [31]. An improved version of Cadzow algorithm has been proposed in [32] and then extended for 2D spectral analysis in [33], in order to estimate the modulation parameters in structured illumination microscopy images. In this paper, the objective is to adapt this 2D spectrum analysis technique in order to estimate the local amplitude, frequency, and orientation of an AM–FM image.

Finally, by combining the proposed variational bi-dimensional EMD with the spectral estimation based on the annihilation property, we propose an efficient adaptive 2D spectral analysis that we call 2D *Prony–Huang Transform* (PHT), whose performances are evaluated on simulated and real data.

Section II is focused on the proposed 2D-EMD, while Section III describes the optimization procedure improving the spectral analysis step. The experimental results and comparisons with the state-of-the art methods are presented in Section IV.

Notations: We denote by $\mathbf{y} = (\mathbf{y}[n, m])_{1 \leq n \leq N_1, 1 \leq m \leq N_2} \in \mathbb{R}^{N_1 \times N_2}$ the matrix expression of an image whose size is $N_1 \times N_2$, the n -th row of the image \mathbf{y} is denoted $\mathbf{y}[n, \cdot] \in \mathbb{R}^{N_2}$, and $\mathbf{y} = (\mathbf{y}[n])_{1 \leq n \leq N} \in \mathbb{R}^N$ is the vector expression of \mathbf{y} , such that $N = N_1 \times N_2$. Let \mathcal{H} denote a real Hilbert space. $\Gamma_0(\mathcal{H})$ models the set of convex, lower semi-continuous, proper functions from \mathcal{H} to $]-\infty, +\infty]$. A proper function is a function that is not equal to $+\infty$ everywhere on its domain. The proximity operator associated to a function $\varphi \in \Gamma_0(\mathcal{H})$ is defined, for every $u \in \mathcal{H}$, as $\text{prox}_\varphi u = \arg \min_{v \in \mathcal{H}} \varphi(v) + \frac{1}{2} \|u - v\|^2$.

Algorithm 1 2D-EMD [14]

```

Initialisation : Set  $\mathbf{a}^{(0)} = \mathbf{x}$ 
For every  $k \in \{1, \dots, K\}$ 
    1) Set  $i=1$ 
    2) Set  $\mathbf{t}^{[i]} = \mathbf{a}^{(k-1)}$ 
    3) Compute the mean envelope of  $\mathbf{t}^{[i]}$  denoted  $\mathbf{m}^{[i]}$ 
    4)  $\mathbf{t}^{[i+1]} = \mathbf{t}^{[i]} - \mathbf{m}^{[i]}$ 
    5) Iterate (i.e.,  $i \leftarrow i + 1$ ) steps 3)-4) until  $\mathbf{m}^{[i]} \equiv 0$ 
    6) Set  $\mathbf{d}^{(k)} = \mathbf{t}^{[i+1]}$ 
    7) Set  $\mathbf{a}^{(k)} = \mathbf{a}^{(k-1)} - \mathbf{d}^{(k)}$ 

```

II. VARIATIONAL 2D-EMD

A. Classical 2D-EMD

We consider an image $\mathbf{x} \in \mathbb{R}^{N_1 \times N_2}$ built as a sum of bidimensional IMFs $(\mathbf{d}^{(k)})_{1 \leq k \leq K}$, and a trend $\mathbf{a}^{(K)} \in \mathbb{R}^{N_1 \times N_2}$, i.e.,

$$\mathbf{x} = \mathbf{a}^{(K)} + \sum_{k=1}^K \mathbf{d}^{(k)}. \quad (1)$$

The 2D-EMD methods [13]–[19] aim at sequentially extracting the IMFs $(\mathbf{d}^{(k)})_{1 \leq k \leq K}$ from the data \mathbf{x} . The usual decomposition process is summarized in Algorithm 1.

One can easily remark that this mode decomposition procedure splits up the trend $\mathbf{a}^{(k-1)}$ into a component having IMF properties, denoted $\mathbf{d}^{(k)}$, and a residual component, denoted $\mathbf{a}^{(k)}$. This decomposition is based on the sifting process (Steps 1)-6) of the algorithm) that consists in iterating the mean envelope removal to $\mathbf{t}^{[i]}$. The idea behind the sifting process is to remove the slower parts of the signal, which are contained in the mean envelopes, in order to extract an oscillating component of zero mean envelope, the IMF $\mathbf{d}^{(k)}$. Note that in step 3), the computation of the mean envelope $\mathbf{m}^{[i]}$ can be obtained through several procedures. For instance, it may denote the mean of the upper and lower envelopes obtained by interpolating the maxima, resp. minima, of $\mathbf{t}^{[i]}$ as proposed in Linderherd *image empirical mode decomposition* (IEMD) [14] or the work by Nunes et al. called *bidimensional empirical mode decomposition* (BEMD) [15]. A faster method to compute the envelopes, based on a Delaunay triangulation of the extrema, is proposed in [16]. Another fast solution based on triangulation is presented in [17], its main difference is that it does not compute envelopes but it directly computes the mean surface from the characteristic points of the image (maxima, minima, and saddle points). In [18] the authors propose to estimate the upper and lower envelopes through a convex optimization procedure in order to avoid over/under shooting problems. Finally, in [34], a tensor-product based method is provided to build the envelopes: interpolation is done separately on rows and columns of the image. Some of these methods are consequently faster and may lead to better performance but they are all based on the sifting principle, which does not have convergence guarantees.

B. Proposed 2D-EMD

As mentioned above, the main limitation of the existing 2D-EMD approaches is the sifting process. In order to avoid

this limitation while keeping the spirit of EMD, we propose to preserve the idea of extracting the trend and the IMF of order k from the trend of order $k - 1$ but we replace the sifting procedure (Steps 1)-6)) by the resolution of a variational approach. The proposed criterion is the following, for every $k \in \{1, \dots, K\}$,

$$(a^{(k)}, d^{(k)}) \in \underset{a \in \mathbb{R}^N, d \in \mathbb{R}^N}{\operatorname{Argmin}} \phi_k(a) + \psi_k(d) + \varphi_k(a, d; a^{(k-1)}) \quad (2)$$

where $\phi_k \in \Gamma_0(\mathbb{R}^N)$ and $\psi_k \in \Gamma_0(\mathbb{R}^N)$ impose respectively the trend and IMF behaviors to the components $a^{(k)}$ and $d^{(k)}$, while $\varphi_k(\cdot, \cdot; a^{(k-1)}) \in \Gamma_0(\mathbb{R}^N \times \mathbb{R}^N)$ aims at modeling that $a^{(k-1)}$ is close to $a^{(k)} + d^{(k)}$.

As proposed in [22] for 1D–EMD, the coupling term is chosen quadratic:

$$(\forall (a, d) \in \mathbb{R}^N \times \mathbb{R}^N) \quad \varphi_k(a, d; a^{(k-1)}) = \|a + d - a^{(k-1)}\|^2. \quad (3)$$

Such a coupling term makes the method robust to sampling artifacts [22].

The smoothness of the trend $a^{(k)}$ is obtained by imposing a constraint on its isotropic total variation. Formally, such a constraint leads to the following choice of ϕ_k , for every $\mathbf{a} \in \mathbb{R}^{N_1 \times N_2}$,

$$\rho^{(k)} \sum_{n=1}^{N_1} \sum_{m=1}^{N_2} \sqrt{|\mathbf{a}[n-1, m] - \mathbf{a}[n, m]|^2 + |\mathbf{a}[n, m-1] - \mathbf{a}[n, m]|^2} \quad (4)$$

with a regularization parameter $\rho^{(k)} > 0$.

At this stage, one can notice the similarities with the texture-geometry decomposition strategies [23]–[25] when $K = 1$. For this class of methods the function ψ_k is chosen to model oscillating signals, for example it can be a ℓ_1 -norm (TV- ℓ_1) [23], or the G -norm that is associated to the Banach space of signals with large oscillations (TV- G) [24], [25], [35]. The texture-geometry decomposition has been designed for extracting a texture from a piece-wise constant image. However, the texture extracted with such a procedure may correspond to any oscillatory behavior and thus can be composed of a sum of two (or more) oscillatory components. For this reason we propose to integrate the IMF properties in the function ψ_k in order to impose a extraction procedure closer to the EMD, which means being able to extract each oscillatory component separately. To achieve this goal, we extend the 1D solution proposed in [22] to the bi-dimensional problem. We describe two solutions that are the *genuine 2D* (G2D) approach, based on 2D local extrema, and the *pseudo 2D* (P2D) approach, where lines, columns, and diagonals extrema are separately constrained (see [13] for a comparison between G2D and P2D approaches in the usual sifting-based EMD procedure).

1) *G2D Approach*: For every $k \in \{1, \dots, K\}$, we identify the P_k extrema of $\mathbf{a}^{(k-1)}$ whose locations are denoted by $\underline{i}^{(k)}[\ell] \in \{1, \dots, N_1\} \times \{1, \dots, N_2\}$. For every $\ell \in \{1, \dots, P_k\}$ such that $\underline{i}^{(k)}[\ell]$ denotes a maxima (resp. a minima), we denote $(\underline{i}_1^{(k)}[\ell], \underline{i}_2^{(k)}[\ell], \underline{i}_3^{(k)}[\ell])$ the locations of the three closest

minima (resp. maxima) in the sense of Euclidean distance. We want to impose that $\mathbf{d}(\underline{i}^{(k)}[\ell])$ is approximatively symmetric with respect to its mirror-point that would be on the minima (resp. maxima) envelope. This condition can be obtained by imposing a constraint on the extrema of \mathbf{d} :

$$\left| \mathbf{d}[\underline{i}^{(k)}[\ell]] + \frac{\alpha_1^{(k)}[\ell] \mathbf{d}[\underline{i}_1^{(k)}[\ell]] + \alpha_2^{(k)}[\ell] \mathbf{d}[\underline{i}_2^{(k)}[\ell]] + \alpha_3^{(k)}[\ell] \mathbf{d}[\underline{i}_3^{(k)}[\ell]]}{\alpha_1^{(k)}[\ell] + \alpha_2^{(k)}[\ell] + \alpha_3^{(k)}[\ell]} \right|, \quad (5)$$

where $(\alpha_j^{(k)}[\ell])_{1 \leq j \leq 3}$ are computed so that $\underline{i}^{(k)}[\ell]$ is the barycenter of the locations $(\underline{i}_j^{(k)}[\ell])_{1 \leq j \leq 3}$ weighted by the $(\alpha_j^{(k)}[\ell])_{1 \leq j \leq 3}$. This penalization can be globally rewritten as:

$$(\forall d \in \mathbb{R}^N) \quad \psi_k(d) = v^{(k)} \|\mathbf{M}_{G2D}^{(k)} d\|_1, \quad (6)$$

where $\mathbf{M}_{G2D}^{(k)} \in \mathbb{R}^{P_k \times N}$ is a sparse matrix modelling the constraint imposed on d , i.e., Eq. (5) can be written $|\mathbf{M}_{G2D}^{(k)}[\ell, \cdot] d|$, where $\mathbf{M}_{G2D}^{(k)}[\ell, \cdot]$ denotes the ℓ -th row of $\mathbf{M}_{G2D}^{(k)}$. More precisely, each row ℓ of $\mathbf{M}_{G2D}^{(k)}$ is sparse and contains 4 non-zero values: 1,

$$\frac{\alpha_1^{(k)}[\ell]}{\alpha_1^{(k)}[\ell] + \alpha_2^{(k)}[\ell] + \alpha_3^{(k)}[\ell]}, \frac{\alpha_2^{(k)}[\ell]}{\alpha_1^{(k)}[\ell] + \alpha_2^{(k)}[\ell] + \alpha_3^{(k)}[\ell]}$$

and

$$\frac{\alpha_3^{(k)}[\ell]}{\alpha_1^{(k)}[\ell] + \alpha_2^{(k)}[\ell] + \alpha_3^{(k)}[\ell]},$$

at locations $\underline{i}^{(k)}[\ell]$, $\underline{i}_1^{(k)}[\ell]$, $\underline{i}_2^{(k)}[\ell]$ and $\underline{i}_3^{(k)}[\ell]$ respectively.

The main difficulty to implement this strategy lies in the detection of extrema locations. Several strategies have been proposed in the literature, for instance in [14] a pixel is considered as a local extremum if its value is maximum/minimum in a 3×3 neighborhood. On the other hand, there are directional strategies that designate a pixel as a maximum (resp. minimum) when its value is greater (resp. lower) than the two closest pixels in any of the 4 principal directions of the image (horizontal, vertical, diagonal, and anti-diagonal). This method makes easier the extraction of oriented textures, that is the reason why we have retained this approach in the present paper. The problem of this second approach lies in the handling of saddle points, which are minima in one direction and maxima in another direction. In this work, we choose not to take these points into account.

2) *P2D Approach*: This solution constrains extrema of each line, column, diagonal and anti-diagonal rather than dealing with local 2D extrema. The proposed strategy is described for the constraint applied on the n -th row. We denote $(n, i^{(k)}[\ell])_{1 \leq \ell \leq P_{k,n}}$ the locations of local maxima/minima in the n -th row of $\mathbf{a}^{(k-1)}$. The condition that imposes a zero mean envelope is

$$\left| \mathbf{d}[n, i^{(k)}[\ell]] + \frac{\alpha_1^{(k)}[\ell] \mathbf{d}[n, i^{(k)}[\ell-1]] + \alpha_2^{(k)}[\ell] \mathbf{d}[n, i^{(k)}[\ell+1]]}{\alpha_1^{(k)}[\ell] + \alpha_2^{(k)}[\ell]} \right|, \quad (7)$$

where $(\alpha_1^{(k)}[\ell], \alpha_2^{(k)}[\ell])$ are computed so that $i^{(k)}[\ell]$ is the barycenter of the locations $(i^{(k)}[\ell - 1], i^{(k)}[\ell + 1])$ weighted by the $(\alpha_1^{(k)}[\ell], \alpha_2^{(k)}[\ell])$. The extrema-based constraint can be written for each row $n \in \{1, \dots, N_1\}$, $|\mathbf{R}_n^{(k)} \mathbf{d}[n, \cdot]^\top|$, where $\mathbf{R}_n^{(k)} \in \mathbb{R}^{P_{k,n} \times N_2}$ denotes the linear combination of some elements of the n -th row $\mathbf{d}[n, \cdot]$ creating a constraint of a zero mean envelope for the component $d^{(k)}$.

Considering the whole image, the constraint can be written $\|\mathbf{R}^{(k)} \mathbf{d}\|_1$ where $\mathbf{R}^{(k)} = \text{diag}(\mathbf{R}_1^{(k)}, \dots, \mathbf{R}_{N_1}^{(k)})$ is a block diagonal matrix, which is highly sparse. We apply the same type of constraint to the columns ($\mathbf{C}^{(k)}$), the diagonals ($\mathbf{D}^{(k)}$), and the anti-diagonals ($\mathbf{A}^{(k)}$) of the image, leading to the penalization:

$$(\forall d \in \mathbb{R}^N) \quad \psi_k(d) = \sum_{l=1}^4 v_l^{(k)} \|\mathbf{M}_l^{(k)} d\|_1 \quad (8)$$

where $\mathbf{M}_1^{(k)} = \mathbf{R}^{(k)}$, $\mathbf{M}_2^{(k)} = \mathbf{C}^{(k)}$, $\mathbf{M}_3^{(k)} = \mathbf{D}^{(k)}$, $\mathbf{M}_4^{(k)} = \mathbf{A}^{(k)}$ denote matrices in $\mathbb{R}^{N \times N}$. In this paper, we used the same regularization parameters for the four directions, i.e., for every $l \in \{1, \dots, 4\}$, $v_l^{(k)} \equiv v^{(k)}$. The main reason of this restriction is to provide a fair comparison with the G2D approach, which uses a single parameter. Moreover, in variational approaches, the question of tuning the parameters is still an open question. Even if interesting solution have been recently provided in the context of image restoration [36]–[39], it is often preferable to have few parameters to tune.

C. Algorithm

For both proposed solutions (G2D–EMD or P2D–EMD), the resulting criteria are convex, non-smooth, and involve sparse (but non-circulant) matrices. Therefore, according to the recent literature in convex optimization, we propose to adapt the primal-dual splitting algorithm proposed in [40] for solving (2). Other efficient primal-dual proximal algorithms such as the one proposed in [41]–[43] could have been employed. In this paper, we will not discuss and compare the performance of these algorithms in order to focus on the performance of the decomposition procedure. However, in our simulation, the algorithm proposed in [36] appears slightly faster in term of convergence of the iterates. The iterations are specified in Algorithm 2 for G2D–EMD, and in Algorithm 3 for P2D–EMD. The difficulties resulting from this minimization problem is first to deal with the Hilbert space $\mathbb{R}^N \times \mathbb{R}^N$ [42], to specify the closed form expression of the proximity operators associated to the ℓ_1 -norm and to the $\ell_{2,1}$ -norm, and to compute the norm of the involved matrices in order to design an efficient algorithm from the computational point of view and to insure convergence. However, for further details on these computations, one could refer to [44]. In order to lighten the notations, we rewrite the total variation penalization as $\phi_k = \rho^{(k)} \|\mathbf{L} \cdot\|_{2,1}$, with $\mathbf{L} = [\mathbf{L}_H^\top \mathbf{L}_V^\top]^\top$ where $\mathbf{L}_H \in \mathbb{R}^{N \times N}$ and $\mathbf{L}_V \in \mathbb{R}^{N \times N}$ denote the matrices associated to the horizontal and vertical finite differences. For the P2D–EMD algorithm, we denote $\mathbf{M}_{P2D}^{(k)} = \text{diag}(\mathbf{M}_1^{(k)}, \mathbf{M}_2^{(k)}, \mathbf{M}_3^{(k)}, \mathbf{M}_4^{(k)})$. Parameters σ and τ are chosen so as to ensure the convergence of the algorithm, see [40] for further details. As the optimization problem is

Algorithm 2 G2D–EMD Algorithm

- Set $\mathbf{a}^{(0)} = \mathbf{x}$,
 For every $k \in \{1, \dots, K\}$
- 1) Compute $\mathbf{M}_{G2D}^{(k)}$ from $\mathbf{a}^{(k-1)}$,
 - 2) Set $\beta = 1 + \|\mathbf{M}_{G2D}^{(k)}\|^2$,
 - 3) Set $\sigma > 0$ and let $\tau = 0.9/(\sigma\beta + 2)^1$,
 - 4) Initialize $a^{[0]}$ and $d^{[0]}$ in \mathbb{R}^N ,
 - 5) Initialize $y_0^{[0]}$ in \mathbb{R}^{2N} and $y_1^{[0]} \in \mathbb{R}^N$
 - 6) For $i = 0, 1, \dots$

$$\begin{cases} a^{[i+1]} = a^{[i]} - 2\tau(a^{[i]} + d^{[i]} - a^{(k-1)}) - \tau \mathbf{L}^\top y_0^{[i]} \\ d^{[i+1]} = d^{[i]} - 2\tau(a^{[i]} + d^{[i]} - a^{(k-1)}) - \tau (\mathbf{M}_{G2D}^{(k)})^\top y_1^{[i]} \\ y_0^{[i+1]} = \text{prox}_{\sigma(\rho^{(k)} \|\cdot\|_{1,2})^*}(y_0^{[i]} + \sigma \mathbf{L}(2a^{[i+1]} - a^{[i]})) \\ y_1^{[i+1]} = \text{prox}_{\sigma(\nu^{(k)} \|\cdot\|_1)^*}(y_1^{[i]} + \sigma \mathbf{M}_{G2D}^{(k)}(2a^{[i+1]} - a^{[i]})) \end{cases}$$
 - 7) Set $d^{(k)} = \lim_{i \rightarrow \infty} d^{[i]}$ and $a^{(k)} = \lim_{i \rightarrow \infty} a^{[i]}$.
-

Algorithm 3 P2D–EMD Algorithm

- Set $\mathbf{a}^{(0)} = \mathbf{x}$,
 For every $k \in \{1, \dots, K\}$
- 1) Compute $(\mathbf{M}_l^{(k)})_{1 \leq l \leq 4}$ from $\mathbf{a}^{(k-1)}$,
 - 2) Set $\beta = 1 + \|\mathbf{M}_{P2D}^{(k)}\|^2$,
 - 3) Set $\sigma > 0$ and let $\tau = 0.9/(\sigma\beta + 2)^1$,
 - 4) Initialize $a^{[0]}$ and $d^{[0]}$ in \mathbb{R}^N ,
 - 5) Initialize $y_0^{[0]}$ in \mathbb{R}^{2N} and $y_l^{[0]} \in \mathbb{R}^N$ for $l = 1, \dots, 4$.
 - 6) For $i = 0, 1, \dots$

$$\begin{cases} a^{[i+1]} = a^{[i]} - 2\tau(a^{[i]} + d^{[i]} - a^{(k-1)}) - \tau \mathbf{L}^\top y_0^{[i]} \\ d^{[i+1]} = d^{[i]} - 2\tau(a^{[i]} + d^{[i]} - a^{(k-1)}) - \tau \sum_{l=1}^4 (\mathbf{M}_l^{(k)})^\top y_l^{[i]} \\ y_0^{[i+1]} = \text{prox}_{\sigma(\rho^{(k)} \|\cdot\|_{1,2})^*}(y_0^{[i]} + \sigma \mathbf{L}(2a^{[i+1]} - a^{[i]})) \\ \text{For } l = 1, \dots, 4 \\ \quad | \quad y_l^{[i+1]} = \text{prox}_{\sigma(\nu_l^{(k)} \|\cdot\|_1)^*}(y_l^{[i]} + \sigma \mathbf{M}_l^{(k)}(2a^{[i+1]} - a^{[i]})) \end{cases}$$
 - 7) Set $d^{(k)} = \lim_{i \rightarrow \infty} d^{[i]}$ and $a^{(k)} = \lim_{i \rightarrow \infty} a^{[i]}$.
-

convex, the initialization of variables $a^{[0]}$, $d^{[0]}$, $y_0^{[0]}$ and $y_1^{[0]}$ does not impact the solution. For the sake of simplicity we initialize them to zero.

III. SPECTRAL ANALYSIS

The previous section was dedicated to methods to extract 2D IMFs. In this section, we now focus on the estimation of the instantaneous frequency, amplitude, and orientation of each IMF. After a short review of monogenic analysis, usually employed for analysing 2D IMFs [8], we propose a new 2D spectral analysis method based on Prony annihilation property.

A. 2D Spectral Estimation Based on Monogenic Signal

We first recall that for a given real-valued 1D signal $d \in \mathbb{R}^N$, the associated analytic signal $d_a \in \mathbb{C}^N$, which by definition involves the signal itself and its Hilbert transform, can also be written under a polar form involving instantaneous phase $\chi \in \mathbb{R}^N$ and amplitude $\alpha \in \mathbb{R}^N$ such as:

$$d_a = d + j\mathcal{H}(d) = \alpha e^{j\chi}, \quad (9)$$

¹It has been proved in [40] that the condition on τ and σ to ensure the weak convergence of the algorithm is $\tau < 1/(\sigma\beta + 2)$.

where $\mathcal{H}(d)$ is the Hilbert transform of d , which consists in a convolution by an all pass filter h characterized by its transfer function $H_\omega = -j\omega/|\omega|$. These two formulations make easy the computation of the instantaneous amplitude and the instantaneous phase as the absolute value of the analytic signal and its argument.

The monogenic analysis is a 2D extension of spectral analysis based on the analytic signal. It is based on the Riesz transform, a natural 2D extension of the Hilbert transform [11]. The Riesz transform of a 2D signal \mathbf{d} can be expressed as $\mathbf{d}_r = (\mathbf{d}_1, \mathbf{d}_2) = (\mathbf{h}_1 * \mathbf{y}, \mathbf{h}_2 * \mathbf{y})$, where the filters $(\mathbf{h}_l)_{1 \leq l \leq 2}$ are characterized by their 2D transfer functions $(\mathbf{H}_l)_{\underline{\omega}} = -j\omega_l/\|\underline{\omega}\|$ with $\underline{\omega} = (\omega_1, \omega_2)$. Based on the Riesz transform, the monogenic signal is the counterpart in 2D of the analytic signal defined as a three-component signal $\mathbf{d}_m = (\mathbf{d}, \mathbf{d}_1, \mathbf{d}_2)$ [11]. Similarly to the analytic signal, the monogenic signal enables to compute easily the local amplitude, phase, and orientation at each pixel through the relations, for every $(n, m) \in \{1, \dots, N_1\} \times \{1, \dots, N_2\}$,

$$\begin{aligned} \alpha[n, m] &= \sqrt{(\mathbf{d}[n, m])^2 + (\mathbf{d}_1[n, m])^2 + (\mathbf{d}_2[n, m])^2} \\ \chi[n, m] &= \arctan\left(\frac{\sqrt{(\mathbf{d}_1[n, m])^2 + (\mathbf{d}_2[n, m])^2}}{\mathbf{d}[n, m]}\right) \\ \theta[n, m] &= \arctan(\mathbf{d}_2[n, m]/\mathbf{d}_1[n, m]). \end{aligned} \quad (10)$$

The local frequency $\eta[n, m]$ is then obtained by differentiating the local phase $\chi[n, m]$ along the direction given by the orientation $\theta[n, m]$, see [12] for further details.

The estimation of the orientation proposed in (10) lacks of robustness because it does not take into account the orientation of neighboring pixels. Unser *et al.* [12] derived an improved estimation based on a minimization procedure including a smoothness neighborhood constraint. It consists in estimating the local orientation which maximizes the directional Hilbert transform over a local neighborhood. To sum up, this optimization problem can be written as the maximization of a quadratic form, which leads to an eigenvalue problem on a matrix of size 2×2 . The eigenvector corresponding to the largest eigenvalue gives the local orientation $\theta[n, m]$ inside the neighborhood, while the difference between the two eigenvalues, normalized to lie in the range $[0, 1]$, gives a coherency index $\lambda[n, m]$. The coherency index models the degree of directionality of the local neighborhood and gives a general reliability index of the estimation: a high coherency index (close to 1) means that pixels into the neighborhood have a similar orientation, while a low coherency index means that there is no privileged orientation into the neighborhood, which means the robust orientation estimation is not reliable.

B. 2D Spectral Analysis Based on the Annihilation Property

The monogenic analysis is efficient for the analysis of instantaneous amplitudes and orientations but unfortunately fails for the frequency estimation, as we will see in Section IV. In this section, we propose an alternative method, based on the annihilation property of a discrete cosine function. While several papers deal with this problem in 1D [30], [32], [45], the

bi-dimensional cosine estimation is still challenging. Recently, in the context of structured illumination microscopy, an efficient 2D spectral estimation strategy has been proposed in order to estimate the global modulation parameters [33]. While in structured illumination microscopy the modulation is uniform through the image, in the present context the modulation may vary from a location to another. For this reason, we propose to adapt the spectral strategy proposed in [33] in order to locally estimate the amplitudes, phases, and orientations of the IMFs. There exists several other spectral analysis methods such as MUSIC [46], ESPRIT [47], MODE [48], [49], WSF [50], which are based on the splitting of the autocorrelation matrix of data into a signal and a noise subspaces. MODE and WSF are widely used in sensor array estimation, they are fast, optimal for large sample data and efficient to separate highly correlated sources. However, these methods are statistically optimal for large sample data. Indeed, these methods are based on an estimate of the data autocorrelation matrix, which needs a large set of samples to be consistent. In this work, we perform local spectral estimation on small patches and therefore we need a method that is particularly efficient for dealing with the limited information.

1) An IMF is Locally a Cosine Function: For every $k \in \{1, \dots, K\}$, we divide the k -th estimated IMF $\mathbf{d}^{(k)}$ into square patches of size $\bar{N}^{(k)}$, i.e.,

$$\left(\forall (\bar{n}, \bar{m}) \in \{1, \dots, \left\lfloor \frac{N_1}{\bar{N}^{(k)}} \right\rfloor\} \times \{1, \dots, \left\lfloor \frac{N_2}{\bar{N}^{(k)}} \right\rfloor\} \right),$$

$$\mathbf{p}_{\bar{n}, \bar{m}}^{(k)} = (\mathbf{d}^{(k)})_{(n, m) \in \mathcal{N}_{\bar{n}, \bar{m}}^{(k)}} \quad (11)$$

where

$$\begin{aligned} \mathcal{N}_{\bar{n}, \bar{m}}^{(k)} &= \{(n, m) \in \{(\bar{n} - 1)\bar{N}^{(k)} + 1, \dots, \bar{n}\bar{N}^{(k)}\} \\ &\quad \times \{(\bar{m} - 1)\bar{N}^{(k)} + 1, \dots, \bar{m}\bar{N}^{(k)}\}\} \end{aligned} \quad (12)$$

and we locally model it by a discrete cosine function that is, for every $(n', m') \in \{1, \dots, \bar{N}^{(k)}\} \times \{1, \dots, \bar{N}^{(k)}\}$,

$$\mathbf{p}_{\bar{n}, \bar{m}}^{(k)}[n', m'] \approx \alpha_{\bar{n}, \bar{m}}^{(k)} \cos(2\pi \xi_{\bar{n}, \bar{m}}^{(k)} n' + 2\pi \zeta_{\bar{n}, \bar{m}}^{(k)} m' + \nu_{\bar{n}, \bar{m}}^{(k)}) \quad (13)$$

where $\alpha_{\bar{n}, \bar{m}}^{(k)}$ models the local amplitude for the patch (\bar{n}, \bar{m}) of the k -th IMF, while $\xi_{\bar{n}, \bar{m}}^{(k)}$ and $\zeta_{\bar{n}, \bar{m}}^{(k)}$ are respectively the local frequencies toward lines and columns. Then, the local frequency and orientation are respectively given by:

$$\eta_{\bar{n}, \bar{m}}^{(k)} = \sqrt{(\xi_{\bar{n}, \bar{m}}^{(k)})^2 + (\zeta_{\bar{n}, \bar{m}}^{(k)})^2}, \quad (14)$$

and

$$\theta_{\bar{n}, \bar{m}}^{(k)} = \arctan(\xi_{\bar{n}, \bar{m}}^{(k)} / \zeta_{\bar{n}, \bar{m}}^{(k)}). \quad (15)$$

The problem is then to estimate the parameters $\alpha^{(k)}, \xi^{(k)}, \zeta^{(k)}, \nu^{(k)}$ which best fit the data $\mathbf{p}^{(k)}$.

2) Principle of Annihilation Property in 1D: For every $n' \in \{1, \dots, \bar{N}\}$ with $\bar{N} \geq 3$, a 1D discrete cosine function $p[n'] = \alpha \cos(2\pi \xi n' + \nu)$ can be written as a sum of two complex exponentials. Thus, according to the annihilation

property [30], the sequence $(p[n'])_{1 \leq n' \leq \bar{N}}$ admits an annihilating filter $f = (f[k])_{0 \leq k \leq 2}$ which satisfies:

$$(\forall n' = \{3, \dots, \bar{N}\}) \sum_{k=0}^2 f[k]p[n' - k] = 0, \quad (16)$$

and has the following Z-transform:

$$F(z) = f[0] + f[1]z^{-1} + f[2]z^{-2} \quad (17)$$

$$= f[0](1 - e^{-j2\pi\xi}z^{-1})(1 - e^{+j2\pi\xi}z^{-1}) \quad (18)$$

that means $f[0] = f[2]$ (i.e., f is symmetric) and $f[1] = -f[2](e^{j2\pi\xi} + e^{-j2\pi\xi})$. It is then straightforward to compute α , ξ , and v from the annihilating filter. Indeed, according to Eq. (18), the roots of the polynomial $F(z)$ are on the unit complex circle and are $e^{-j2\pi\xi}$ and $e^{+j2\pi\xi}$, which leads to the value of ξ . Then, by linear regression, we retrieve the complex amplitude αe^{jv} . Consequently, the main difficulty consists in estimating the annihilating filter f .

First, it can be shown easily that, if $f = (f[0], f[1], f[2])$ is an annihilating filter of the cosine function p , any non trivial filter $f' = (f'[k])_{0 \leq k \leq L}$, where $2 \leq L \leq \bar{N} - 3$, is also an annihilating filter of p if the roots of f are roots of f' . The inverse is true: if f' is a non trivial annihilating filter of p , then the roots of f are roots of f' . The annihilating equation can then be rewritten as:

$$(\forall n' = \{L + 1, \dots, \bar{N}\}) \sum_{k=0}^L f'[k]p[n' - k] = 0, \quad (19)$$

or equivalently in the matrix form, $T_L(p)f' = 0$, with

$$T_L(p) = \begin{pmatrix} p[\bar{N} - L] & \dots & p[\bar{N} - 1] & p[\bar{N}] \\ p[\bar{N} - L - 1] & \dots & p[\bar{N} - 2] & p[\bar{N} - 1] \\ \vdots & \vdots & \vdots & \vdots \\ p[1] & \dots & p[L] & p[L + 1] \\ \hline p[L + 1] & \dots & p[2] & p[1] \\ \vdots & \vdots & \vdots & \vdots \\ p[\bar{N}] & \dots & p[\bar{N} - L + 1] & p[\bar{N} - L] \end{pmatrix} \quad (20)$$

where $T_L(p) \in \mathbb{R}^{2(\bar{N}-L) \times (L+1)}$. The symmetrization of $T_L(p)$ ensures the symmetry of the filter.

Second, according to [30], p is a sinusoid if and only if, for any L , $T_L(p)$ has a rank of two. The simplest annihilating filter h is obtained from $T_2(p)$ by considering its right singular vector corresponding to the 3rd singular value which is zero (due to $L = 2$ and that the rank of $T_2(p)$ is 2, the two others singular values are non-zero).

This strategy cannot be applied directly on degraded data. In [30] and [32], the authors propose an iterative strategy to estimate the matrix $\hat{T} = T_L(\hat{p})$ of rank 2, where \hat{p} denotes the denoised sinusoidal signal that is the closest from p . Consequently, the denoising strategy consists in solving the following structured low-rank approximation (SLRA) problem:

$$\hat{T} \in \underset{\substack{T \in \mathcal{T} \\ T \in \mathcal{R}_2}}{\operatorname{Argmin}} \|\sqrt{P} \circ (T - T_L(p))\|_F^2, \quad (21)$$

Algorithm 4 Spectral Estimation Algorithm

For $\bar{n} = 1, \dots, \lfloor N_1/\bar{N}^{(k)} \rfloor$, $\bar{m} = 1, \dots, \lfloor N_2/\bar{N}^{(k)} \rfloor$,

STEP 1 – Initialization
Choose the parameters $\mu > 0$, $\gamma \in]0, 1[$
Set the initial estimates $U^{(0)}, V^{(0)}, S^{(0)}, T^{(0)}$

STEP 2 – Iteration : for $l = 0, 1, \dots$

$$U^{(l+1)} = P_{\mathcal{R}_2} \left(S^{(l)} + \gamma(U^{(l)} - S^{(l)}) \right. \\ \left. - \mu P \circ (U^{(l)} - U_{L^{(k)}}(P_{\bar{n}, \bar{m}}^{(k)})) \right)$$

$$V^{(l+1)} = P_{\mathcal{R}_2} \left(T^{(l)} + \gamma(V^{(l)} - T^{(l)}) \right. \\ \left. - \mu P \circ (V^{(l)} - V_{L^{(k)}}(P_{\bar{n}, \bar{m}}^{(k)})) \right)$$

$$(S^{(l+1)}, T^{(l+1)}) = (S^{(l)}, T^{(l)}) - (U^{(l+1)}, V^{(l+1)}) \\ + P_{\mathcal{T}^{(k)}}(2(U^{(l+1)}, V^{(l+1)}) - (S^{(l)}, T^{(l)}))$$

STEP 3 – Parameters estimation :
 $\hat{U}_{\bar{n}, \bar{m}}^{(k)} = U^{(l)}$, $\hat{V}_{\bar{n}, \bar{m}}^{(k)} = V^{(l)}$
Compute $\hat{p}_{\bar{n}, \bar{m}}^{(k)}$ from $\hat{U}_{\bar{n}, \bar{m}}^{(k)}$ or $\hat{V}_{\bar{n}, \bar{m}}^{(k)}$
Compute the annihilating filters $\hat{f}_{\bar{n}, \bar{m}}^{(k)}$ and $\hat{g}_{\bar{n}, \bar{m}}^{(k)}$ from $\hat{p}_{\bar{n}, \bar{m}}^{(k)}$
Compute $\hat{\alpha}_{\bar{n}, \bar{m}}^{(k)}, \hat{\xi}_{\bar{n}, \bar{m}}^{(k)}, \hat{\zeta}_{\bar{n}, \bar{m}}^{(k)}$ from $\hat{f}_{\bar{n}, \bar{m}}^{(k)}$ and $\hat{g}_{\bar{n}, \bar{m}}^{(k)}$
Compute $\hat{\eta}_{\bar{n}, \bar{m}}^{(k)}, \hat{\theta}_{\bar{n}, \bar{m}}^{(k)}$ from $\hat{\xi}_{\bar{n}, \bar{m}}^{(k)}$ and $\hat{\zeta}_{\bar{n}, \bar{m}}^{(k)}$

where $P \in \mathbb{R}^{2(\bar{N}-L) \times (L+1)}$ denotes a weighting matrix whose entries are inversely equal to the number of times where the entry models the same element, \circ is the entrywise product, $\|\cdot\|_F$ is the Frobenius norm. \mathcal{T} is the set of matrices $\mathcal{T} = \{(T_L(c)) : c \in \mathbb{R}^N\}$, and \mathcal{R}_2 is the set of matrices with a maximal rank of 2. The problem can be solved with an iterative primal-dual algorithm as proposed in [32]. L is chosen so that $T_L(p)$ is as close to a square matrix as possible, in order to improve the convergence speed of the algorithm.

3) Spectral Analysis of IMFs: The procedure described previously has been extended for 2D spectral analysis in [33] when the modulation is uniform through the whole image. In our work, in the scope of providing an adaptive 2D spectral analysis method designed for nonstationary images, we will estimate amplitudes, frequencies and orientations *locally*. The idea is then to apply the method proposed in [33] on the local patches $\mathbf{p}_{\bar{n}, \bar{m}}^{(k)} \in \mathbb{R}^{\bar{N}^{(k)} \times \bar{N}^{(k)}}$.

In the situation where the (k, \bar{n}, \bar{m}) -th patch $\mathbf{p}_{\bar{n}, \bar{m}}^{(k)}$ is a strict sinusoid, there exists two annihilating filters $\mathbf{f}_{\bar{n}, \bar{m}}^{(k)}$ and $\mathbf{g}_{\bar{n}, \bar{m}}^{(k)}$, both symmetric and of size 3, which annihilate respectively the rows and the columns of the patch. The roots of the Z-transform of $\mathbf{f}_{\bar{n}, \bar{m}}^{(k)}$ are $e^{-j2\pi\xi_{\bar{n}, \bar{m}}^{(k)}}$ and $e^{+j2\pi\xi_{\bar{n}, \bar{m}}^{(k)}}$, which leads to $\xi_{\bar{n}, \bar{m}}^{(k)}$ as it is chosen positive. The same calculation with $\mathbf{g}_{\bar{n}, \bar{m}}^{(k)}$ gives $\pm\xi_{\bar{n}, \bar{m}}^{(k)}[\bar{n}, \bar{m}]$, the sign of $\xi_{\bar{n}, \bar{m}}^{(k)}$ has to be disambiguated in order to compute the orientation. Finally, a linear regression gives us the complex amplitude $\alpha_{\bar{n}, \bar{m}}^{(k)} e^{jv_{\bar{n}, \bar{m}}^{(k)}}$ and disambiguates the sign of $\xi_{\bar{n}, \bar{m}}^{(k)}$, see [32] for more details.

The IMFs extracted with the EMD procedures described in Section II do not behave exactly like a local cosine. Consequently, a SLRA based procedure is used in order to achieve an efficient 2D-block spectral estimation. The problem to solve is:

$$(\hat{U}_{\bar{n}, \bar{m}}^{(k)}, \hat{V}_{\bar{n}, \bar{m}}^{(k)}) \in \underset{\substack{(U, V) \in \mathcal{T}^{(k)} \\ U \in \mathcal{R}_2 \\ V \in \mathcal{R}_2}}{\operatorname{Argmin}} \frac{\|\sqrt{P} \circ (U - U_{L^{(k)}}(P_{\bar{n}, \bar{m}}^{(k)}))\|_F^2}{\|\sqrt{P} \circ (V - V_{L^{(k)}}(P_{\bar{n}, \bar{m}}^{(k)}))\|_F^2} \quad (22)$$

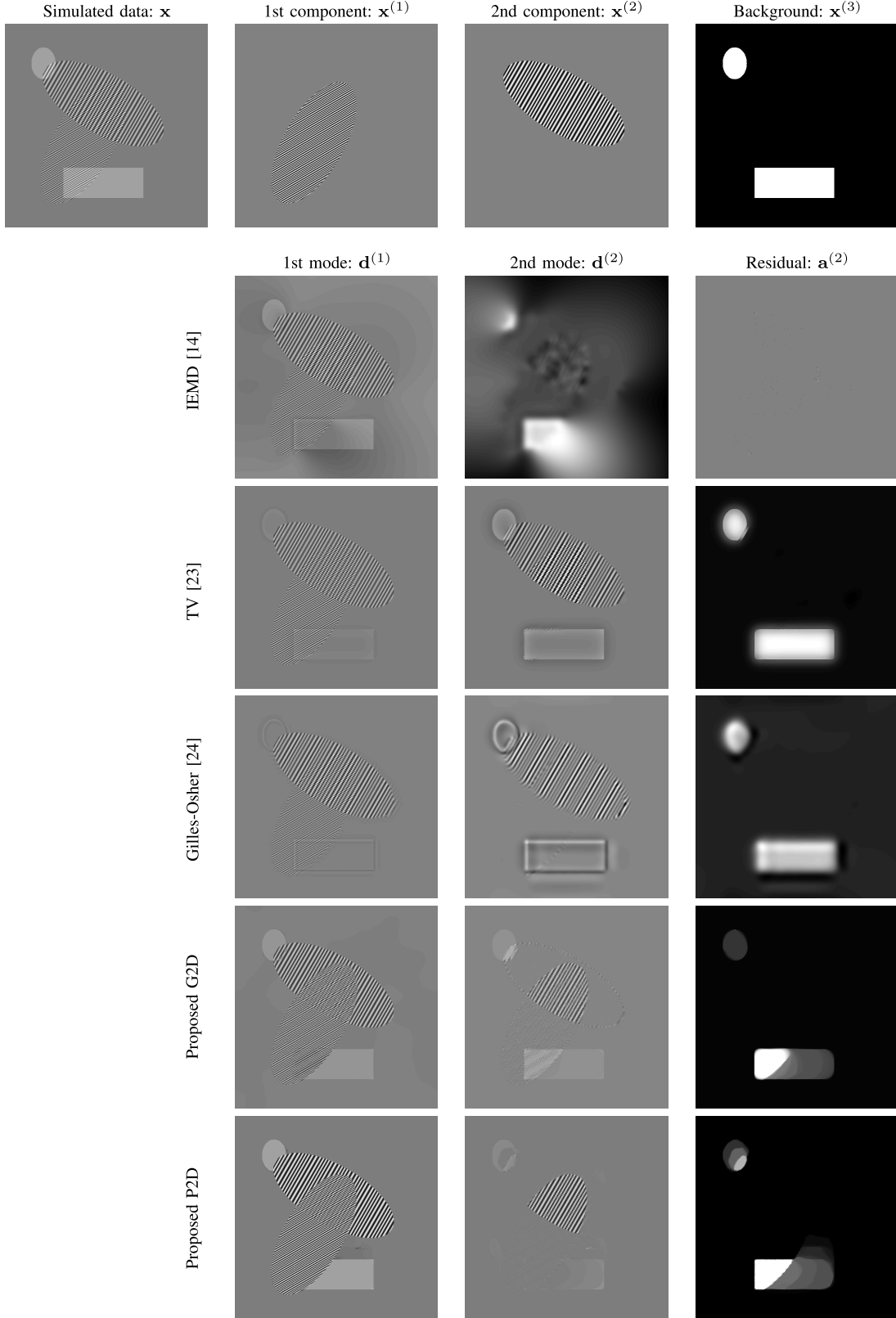


Fig. 1. Decomposition of the simulated data obtained with different methods. 1st row: Simulated data. 2nd row: Image Empirical Mode Decomposition [14]. 3rd row: Total Variation based decomposition [23], 4th row: Gilles-Osher based decomposition [24], 5th row: G2D–EMD, 6th row: P2D–EMD. On 1st row, from the left to the right the columns present \mathbf{x} , $\mathbf{x}^{(1)}$, $\mathbf{x}^{(2)}$, $\mathbf{x}^{(3)}$. From the left to the right the columns present $\mathbf{d}^{(1)}$, $\mathbf{d}^{(2)}$ and $\mathbf{a}^{(2)}$.

where $\mathcal{T}^{(k)}$ is the set $\mathcal{T}^{(k)} = \{(\mathbf{U}_{L^{(k)}}(c), \mathbf{V}_{L^{(k)}}(c)) : c \in \mathbb{R}^{\bar{N}^{(k)} \times \bar{N}^{(k)}}\}$, and $\mathbf{U}_{L^{(k)}}$ and $\mathbf{V}_{L^{(k)}}$ map respectively the lines and columns of a patch of size $\bar{N}^{(k)} \times \bar{N}^{(k)}$ into a centro-symmetric

Toeplitz matrix of size $2\bar{N}^{(k)}(\bar{N}^{(k)} - L^{(k)}) \times (L^{(k)} + 1)$. See [33] for more details on the construction of $\mathbf{U}_{L^{(k)}}(\mathbf{p}_{\bar{n}, \bar{m}}^{(k)})$ and $\mathbf{V}_{L^{(k)}}(\mathbf{p}_{\bar{n}, \bar{m}}^{(k)})$. The weighting matrix \mathbf{P} of size

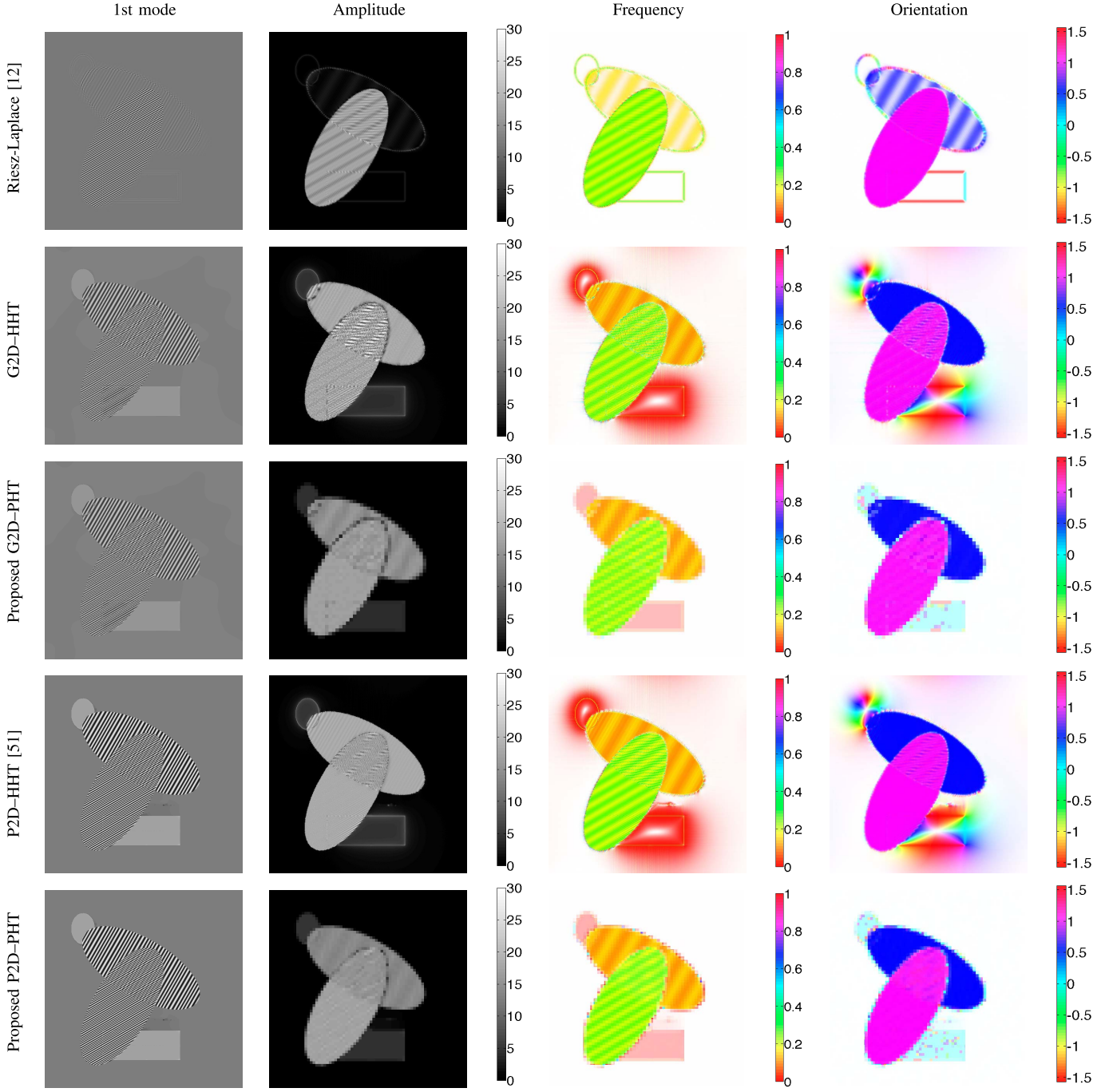


Fig. 2. Spectral analysis on the 1st mode using different methods. 1st row: Riesz-Laplace [12]. 2nd row: G2D-HHT (G2D-EMD + monogenic analysis). 3rd row: G2D-PHT (G2D-EMD + annihilation based spectral analysis). 4th row: P2D-HHT (P2D-EMD + monogenic analysis) [51]. 5th row: P2D-PHT (P2D-EMD + annihilation based spectral analysis). From left to right: mode $\mathbf{d}^{(1)}$, amplitude $\alpha^{(1)}$, frequency $\eta^{(1)}$ and orientation $\theta^{(1)}$.

$2\bar{N}^{(k)}(\bar{N}^{(k)} - L^{(k)}) \times (L^{(k)} + 1)$ is defined similarly as for the original 1D SLRA.

4) *Algorithm for Analysing IMFs:* Similarly as in [33], the SLRA problem is solved with a primal-dual algorithm, which alternates between a gradient descent with respect to the cost function (the squared Frobenius norm) with projections $\mathcal{P}_{\mathcal{T}^{(k)}}$ and $\mathcal{P}_{\mathcal{R}_2}$ to enforce the constraints. $\mathcal{P}_{\mathcal{T}^{(k)}}$ is the orthogonal projection of a pair of matrices (U, V) on $\mathcal{T}^{(k)}$ that consists in averaging the coefficients of U and V corresponding to the same pixel of the image. $\mathcal{P}_{\mathcal{R}_2}$ is the orthogonal projection on the set of matrices of rank at most 2, it is done by SVD truncation, that consists to set to zero all singular

values except the two largest ones. The algorithm is described in Algorithm 4.

5) *Coherency Index:* Inspired by [12], we introduce a new coherency index, defined as $\widehat{\lambda} = \{\widehat{\lambda}_{\bar{n}, \bar{m}}^{(k)}\}_{k, \bar{n}, \bar{m}} \in [0; 1]$ in order to provide a degree of quality of the spectral estimation. For every (k, \bar{n}, \bar{m}) , $\widehat{\lambda}_{\bar{n}, \bar{m}}^{(k)}$ is given by the sum of the two higher singular values of $\widehat{\mathbf{p}}_{\bar{n}, \bar{m}}^{(k)}$, normalized to have an index between 0 and 1. $\widehat{\lambda}$, which is highly linked to the amplitude $\widehat{\alpha}$, informs us about the local oscillatory character of data: it is higher on oscillating parts of the signal, and lower on non-oscillating parts and parts containing only noise.

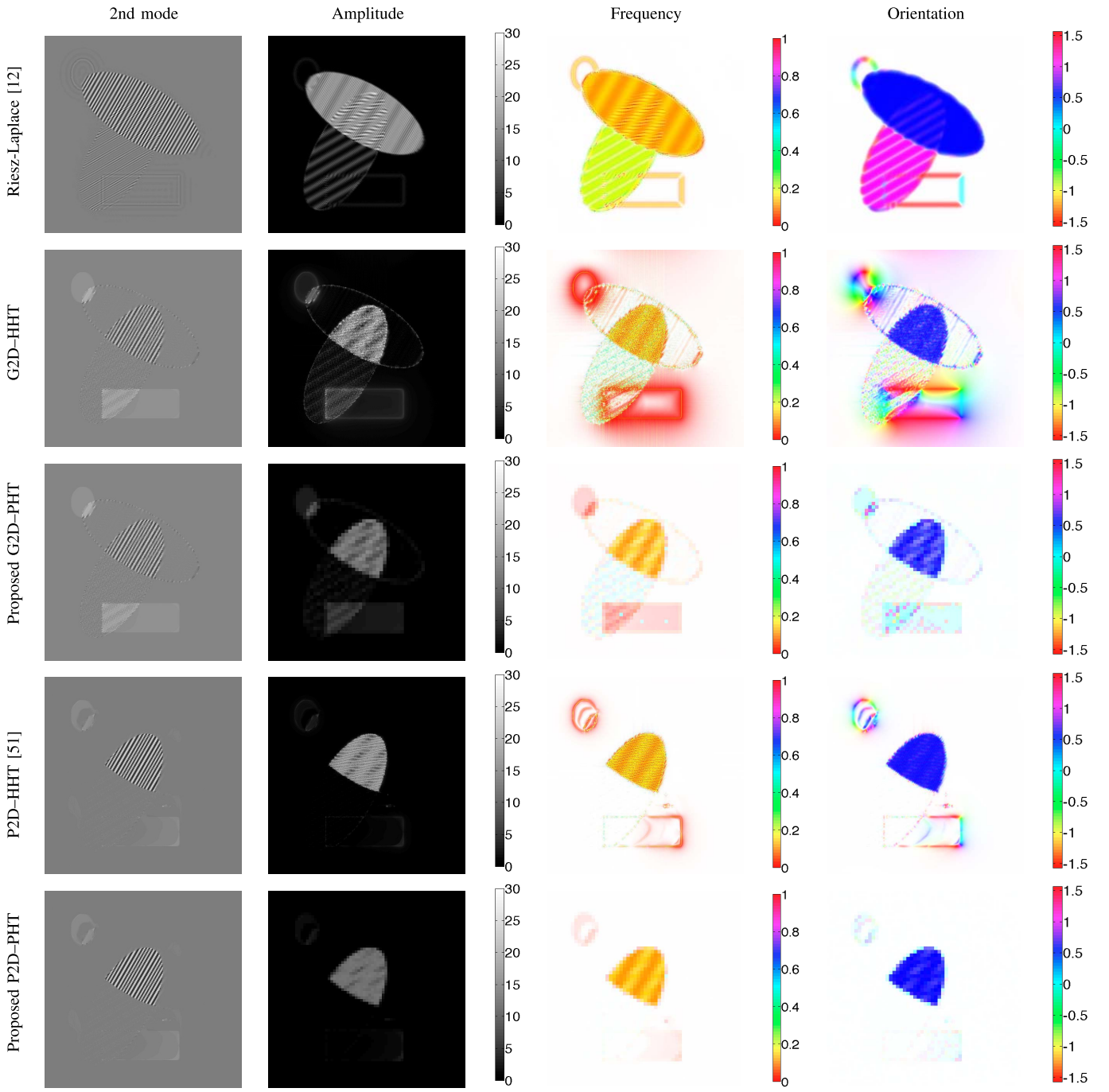


Fig. 3. Spectral analysis on 2nd mode using different methods. 1st row: Riesz-Laplace [12]. 2nd row: G2D–HHT (G2D–EMD + monogenic analysis). 3rd row: G2D–PHT (G2D–EMD + annihilation based spectral analysis). 4th row: P2D–HHT (P2D–EMD + monogenic analysis) [51]. 5th row: P2D–PHT (P2D–EMD + annihilation based spectral analysis). From left to right: mode $\mathbf{d}^{(2)}$, amplitude $\alpha^{(2)}$, frequency $\eta^{(2)}$ and orientation $\theta^{(2)}$.

6) *Size of the Patches*: The patch size $\bar{N}^{(k)}$ should be chosen so that the IMF can be modeled as a sinusoidal function inside a patch. This means that it should be small enough so that the frequency and orientation can be considered constant inside a patch, and large enough so that each patch contains at least one period of oscillation.

IV. EXPERIMENTS

A. Simulations

The first experiment is on simulated data of size $N = 512 \times 512$, consisting in a sum of two localized texture components $\mathbf{x}^{(1)}$ and $\mathbf{x}^{(2)}$ and a piecewise

constant background $\mathbf{x}^{(3)}$. The background is formed with two piecewise constant patches: one rectangular patch and one ellipsoidal patch. The component $\mathbf{x}^{(1)}$ (resp. $\mathbf{x}^{(2)}$) models a modulated signal of central frequency $\eta_1 = 120/512$ (resp. $\eta_2 = 60/512$).

1) *EMD*: We compare our two variational EMD approaches (G2D–EMD and P2D–EMD) with several state-of-the-art decomposition methods that are (a) a classical 2D–EMD method, image empirical mode decomposition (IEMD) [14], which is a natural 2D extension of EMD based on 2D interpolation of extrema using thin-plate spline, (b) a texture–cartoon decomposition methods based on total

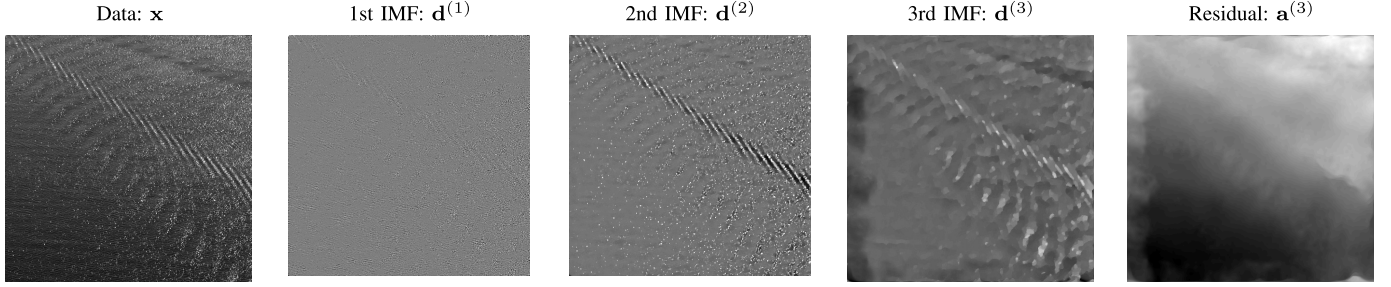


Fig. 4. P2D-EMD decomposition of wake image. 1st IMF: $\rho^{(1)} = 50$, $v^{(1)} = 50$. 2nd IMF: $\rho^{(2)} = 20$, $v^{(2)} = 5$. 3rd IMF: $\rho^{(3)} = 20$, $v^{(3)} = 1$.

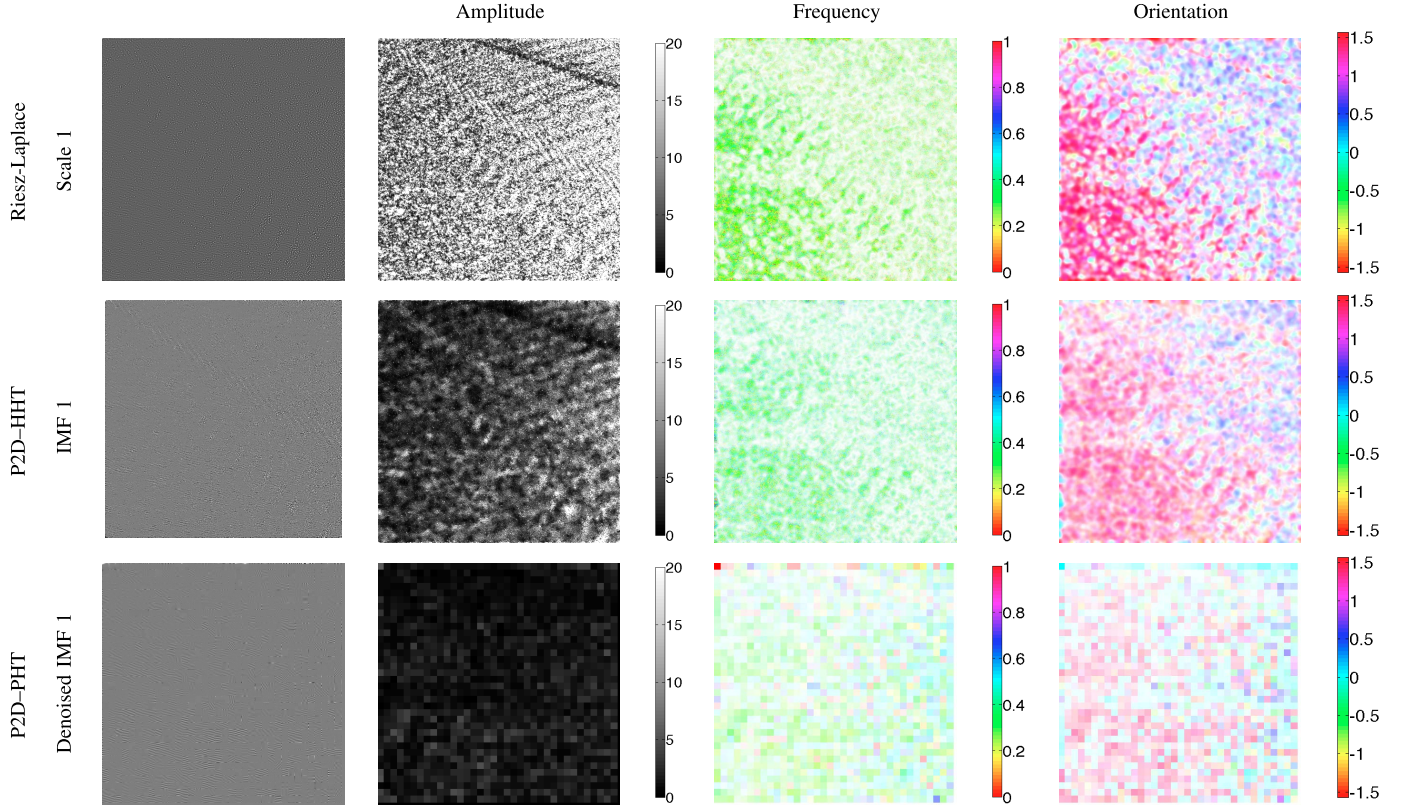


Fig. 5. Spectral analysis on 1st mode of wake image. 1st row: 1st scale of Riesz-Laplace wavelet transform. From left to right: mode $\mathbf{d}^{(1)}$, amplitude $\alpha^{(1)}$, frequency $\eta^{(1)}$ and orientation $\theta^{(1)}$. 2nd row: 1st IMF P2D-HHT. From left to right: mode $\mathbf{d}^{(1)}$, amplitude $\alpha^{(1)}$, frequency $\eta^{(1)}$ and orientation $\theta^{(1)}$. 3rd row: 1st IMF P2D-PHT ($\bar{N}^{(1)} = 14$). From left to right: denoised mode, amplitude $\alpha^{(1)}$, frequency $\eta^{(1)}$ and orientation $\theta^{(1)}$.

variation decomposition [23] and (c) the Gilles-Osher texture-geometry decomposition [24], which is an iterative procedure designed to solve the Meyer G -norm texture-cartoon decomposition problem (similarly to the proposed solution, for both texture-geometry decomposition, we denote $\rho^{(k)}$ the cartoon regularization parameter and $v^{(k)}$ the texture regularization parameter).

In our experiments, the regularization parameters are chosen as follows for G2D-EMD: $\rho^{(1)} = 0.02$, $v^{(1)} = 1000$, $\rho^{(2)} = 0.05$, $v^{(2)} = 1$ while for P2D-EMD, we use $\rho^{(1)} = 0.3$, $v^{(1)} = 0.3$, $\rho^{(2)} = 1$, $v^{(2)} = 0.1$. For Total Variation decomposition method, we set $\rho^{(1)} = 70$ and $\rho^{(2)} = 100$. For Gilles-Osher method, we set $\rho^{(1)} = 10^4$, $v^{(1)} = 10^3$, $\rho^{(2)} = 10$, and $v^{(2)} = 10$. The results are displayed on Fig. 1.

First of all, our method provides a good separation of the different components. It has the expected behaviour of a

2D-EMD, especially the P2D-EMD method: the locally fastest oscillating components are extracted at each step of the decomposition, even if their frequencies are nonstationary. The G2D-EMD approach also gives good results, but the oscillating components are not so perfectly separated. On contrary, the state-of-the-art IEMD does not manage to separate at all the components \mathbf{x}_1 and \mathbf{x}_2 . In comparison with other approaches like texture-cartoon decomposition, the proposed 2D-EMD approach provides more adaptivity and a better management of nonstationary signals. The TV based approach does not give a good separation of the three oscillating components. Gilles-Osher solution is not suited for nonstationary signals: some of the slower part of the frequency modulated component \mathbf{x}_2 is on the 2nd mode, while its faster part is localized on the first mode.

To estimate the computational time of each method, we define a stopping criterion based on the norm of the dif-

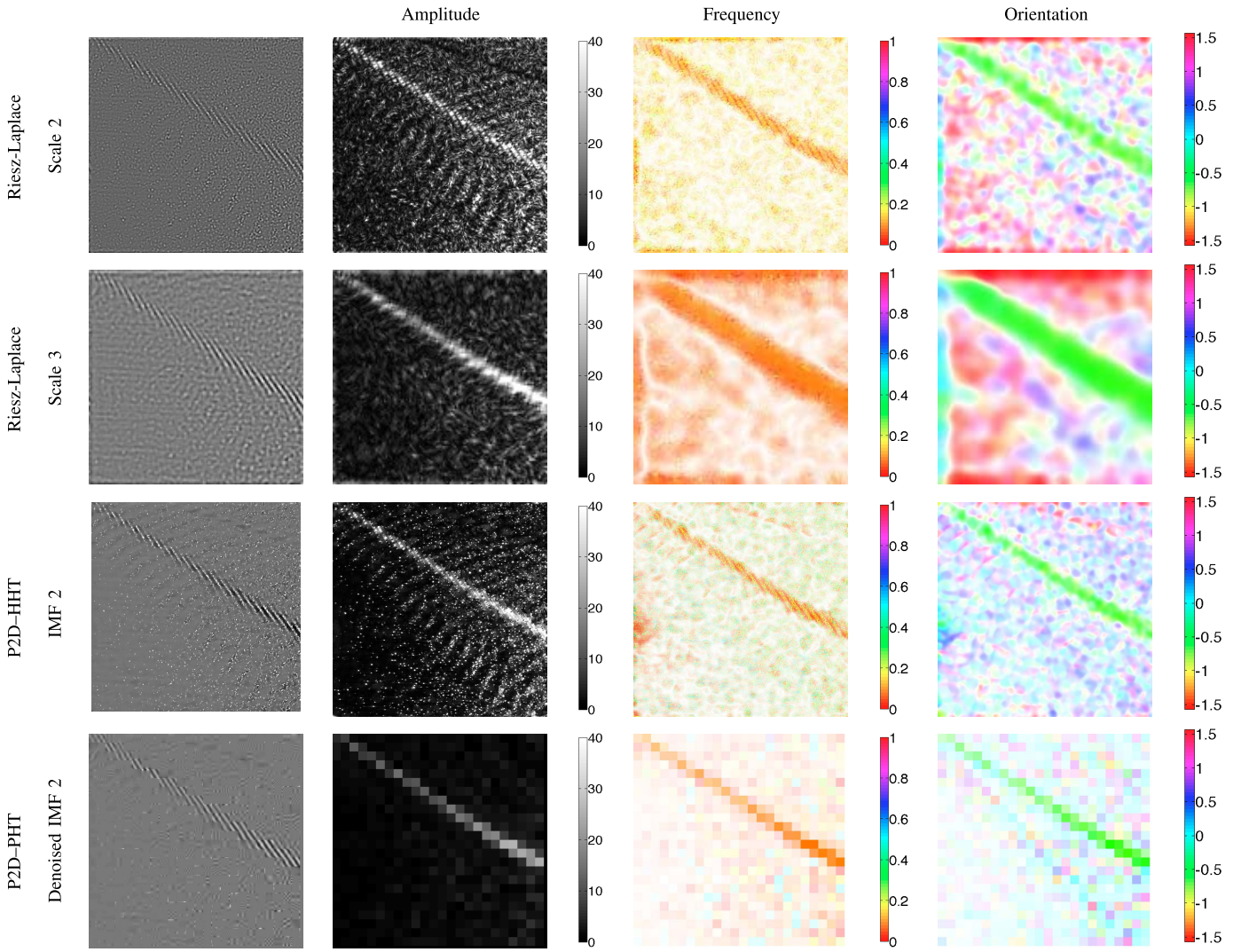


Fig. 6. Spectral analysis on 2nd mode of wake image. 1st row: 2nd scale of Riesz-Laplace wavelet transform. From left to right: mode $\mathbf{d}^{(2)}$, amplitude $\alpha^{(2)}$, frequency $\eta^{(2)}$ and orientation $\theta^{(2)}$. 2nd row: 3rd scale of Riesz-Laplace wavelet transform. From left to right: mode $\mathbf{d}^{(3)}$, amplitude $\alpha^{(3)}$, frequency $\eta^{(3)}$ and orientation $\theta^{(3)}$. 3rd row: 2nd IMF P2D–HHT. From left to right: mode $\mathbf{d}^{(2)}$, amplitude $\alpha^{(2)}$, frequency $\eta^{(2)}$ and orientation $\theta^{(2)}$. 4th row: 2nd IMF P2D–PHT ($\bar{N}^{(2)} = 21$). From left to right: denoised mode, amplitude $\alpha^{(2)}$, frequency $\eta^{(2)}$ and orientation $\theta^{(2)}$.

ference between two successive iterates set to 10^{-6} . The complete decomposition into two modes needs around 3 minutes with TV decomposition, around 6 minutes with Gilles-Osher decomposition, and less than 15 minutes with P2D–EMD. The decomposition using G2D–EMD is substantially longer and takes too much time to reach the stopping criterion, so we have stopped the algorithm after 10^4 iterations. Then, the full decomposition with G2D–EMD takes a little less than 1 hour. P2D–EMD takes a few more time than other state-of-the-art methods, but it is compensated with the better separation performance.

2) *Spectral Analysis*: We perform two types of spectral analysis on the IMFs obtained by G2D–EMD and P2D–EMD. The first approach, that we proposed in [51], is based on a monogenic analysis. We refer to this approach as G2D–HHT and P2D–HHT. On the other hand, the proposed method based on Prony’s annihilation property is referred as G2D–PHT and P2D–PHT. Results on simulations are shown on Figs. 2 and 3. For the annihilation based method, we have chosen $\bar{N}^{(k)} = 7$ for both IMFs. A comparison with the

Riesz-Laplace transform analysis proposed in [12] is also performed. For the three methods, frequency and orientation maps are composed by the coherency index, in order to have better visual results.

The EMD based procedure appears to be more adaptive and better suited for nonstationary data than Riesz-Laplace transform. Moreover, one should notice that the PHT based spectral estimation gives smoother results and performs better for higher order IMFs, especially for the frequency estimation. Indeed, the denoising step of the Prony based estimation achieves a better robustness with respect to errors linked to the EMD decomposition step. The drawbacks of the proposed annihilation based method are the loss of resolution and the computational time.

B. Real Data

The second experiment is performed on a boat wake image.² Regarding the performance of P2D–HHT compared to

²http://www.123rf.com/photo_17188220_fast-boat-in-the-far-blue-sea.html

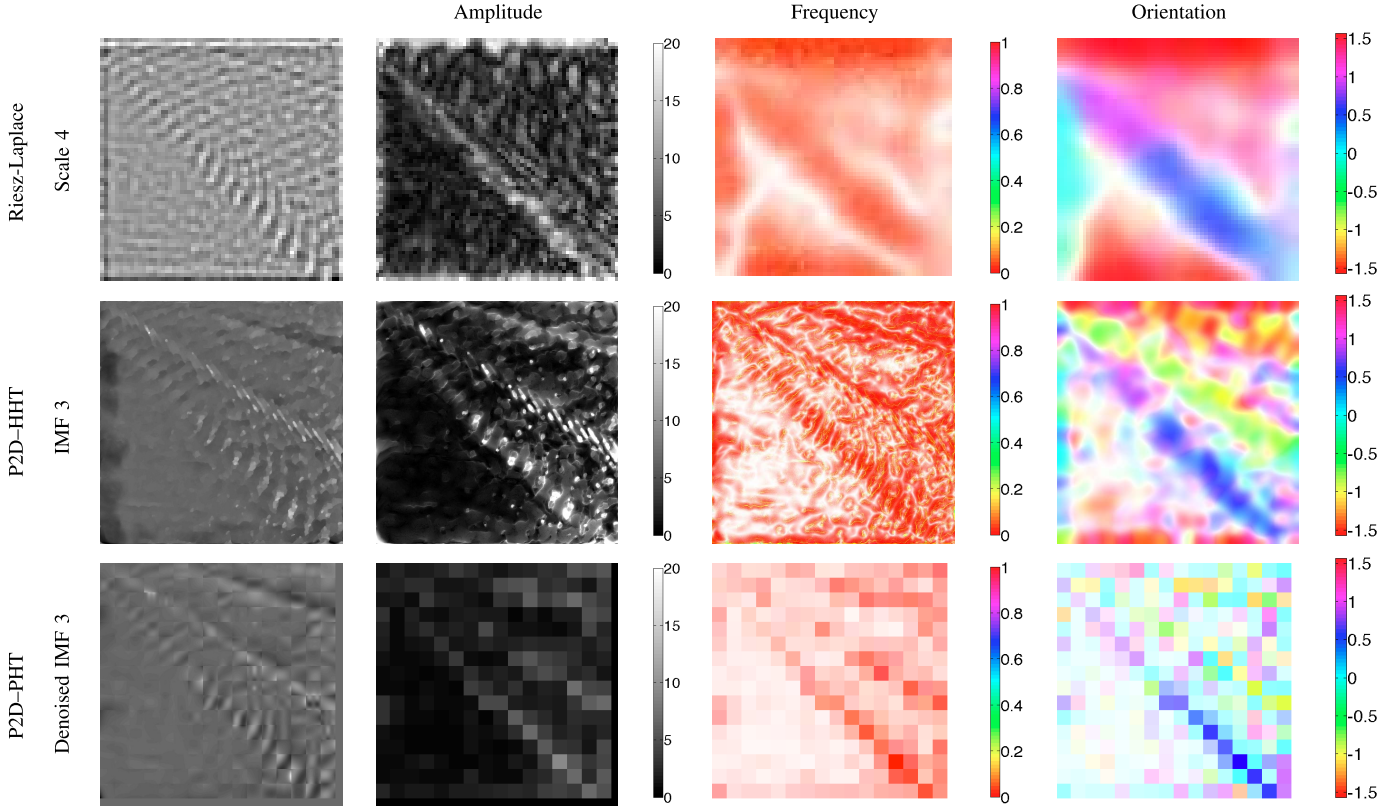


Fig. 7. Spectral analysis on 3rd mode of wake image. 1st row: 4th scale of Riesz-Laplace wavelet transform. From left to right: mode $\mathbf{d}^{(4)}$, amplitude $\alpha^{(4)}$, frequency $\eta^{(4)}$ and orientation $\theta^{(4)}$. 2nd row: 3rd IMF P2D-HHT. From left to right: mode $\mathbf{d}^{(3)}$, amplitude $\alpha^{(3)}$, frequency $\eta^{(3)}$ and orientation $\theta^{(3)}$. 3rd row: 3rd IMF P2D-PHT ($\bar{N}^{(3)} = 31$). From left to right: denoised mode, amplitude $\alpha^{(3)}$, frequency $\eta^{(3)}$ and orientation $\theta^{(3)}$.

G2D-HHT on simulated data, we have decided to focus on this method in our experiments on real data. We compare the results obtained with the proposed P2D-PHT method with P2D-HHT and Riesz-Laplace wavelet transform. The results obtained with the proposed P2D-EMD are shown in Fig. 4. We have used the following optimal parameters: $\rho^{(1)} = 50$, $v^{(1)} = 50$, $\rho^{(2)} = 20$, $v^{(2)} = 5$, $\rho^{(3)} = 20$, $v^{(3)} = 1$. The first IMF contains the fastest small waves. The second IMF contains a slower wave as well as some salt-and-pepper noise, while the third IMF contains the slowest waves. The trend results in the illumination map. The spectral analysis is performed for the three IMFs and the results are displayed in Figs. 5, 6 and 7. For the P2D-PHT, the size of patches has to be chosen so as to be adapted to the frequency of the waves contained in each IMF: a single patch should contain at least one complete period of the wave. Consequently, we have chosen $\bar{N}^{(1)} = 14$, $\bar{N}^{(2)} = 21$ and $\bar{N}^{(3)} = 31$. The Riesz-Laplace transform provides good results but suffers from redundancy between the different scales. For example, the second and third wavelet scales contain the same component. Moreover, the methods based on monogenic analysis (Riesz-Laplace and P2D-HHT) give good results for the orientation estimation but are less performant for frequency estimation. Indeed, the orientation is obtained using a robust neighborhood based estimation method, while the frequency is computed pixel-by-pixel from the monogenic signal, which makes the frequency estimation very sensitive to noise. The

proposed P2D-PHT method appears to be more robust and consequently gives better results for the frequency estimation. The main drawback of the P2D-PHT is the loss of resolution, especially for the coarsest IMF which requires to deal with a large size for patches.

C. Quantitative Evaluation of P2D-EMD

In order to evaluate quantitatively the performance of the method, we performed several tests on synthetic images of size 128×128 :

- Experiment 1 consists in a nonstationary image constituted of the sum of two AM-FM components. The mean frequency of the first component is $f_{c1} = 16/128$, its modulation frequency is $f_{m1} = 4/128$, and its orientation $\theta_1 = \pi/3$. The second component is composed with two AM-FM components placed on each half of the image: an AM-FM component of high frequency on the left half of the image ($f_{c2} = 32/128$, $f_{m2} = 8/128$, $\theta_2 = \pi/4$) and an AM-FM component of low frequency on the right half of the image ($f_{c3} = 4/128$, $f_{m3} = 1/128$, $\theta_3 = \pi/4$).
- Experiment 2 corresponds to a similar configuration as first experiment with a different orientation for the first component ($f_{c1} = 16/128$, $f_{m1} = 4/128$, $\theta_1 = -\pi/3$, $f_{c2} = 32/128$, $f_{m2} = 8/128$, $\theta_2 = \pi/4$, $f_{c3} = 4/128$, $f_{m3} = 1/128$, $\theta_3 = \pi/4$).
- Experiment 3 corresponds to a similar configuration as first experiment with higher frequencies ($f_{c1} = 32/128$,

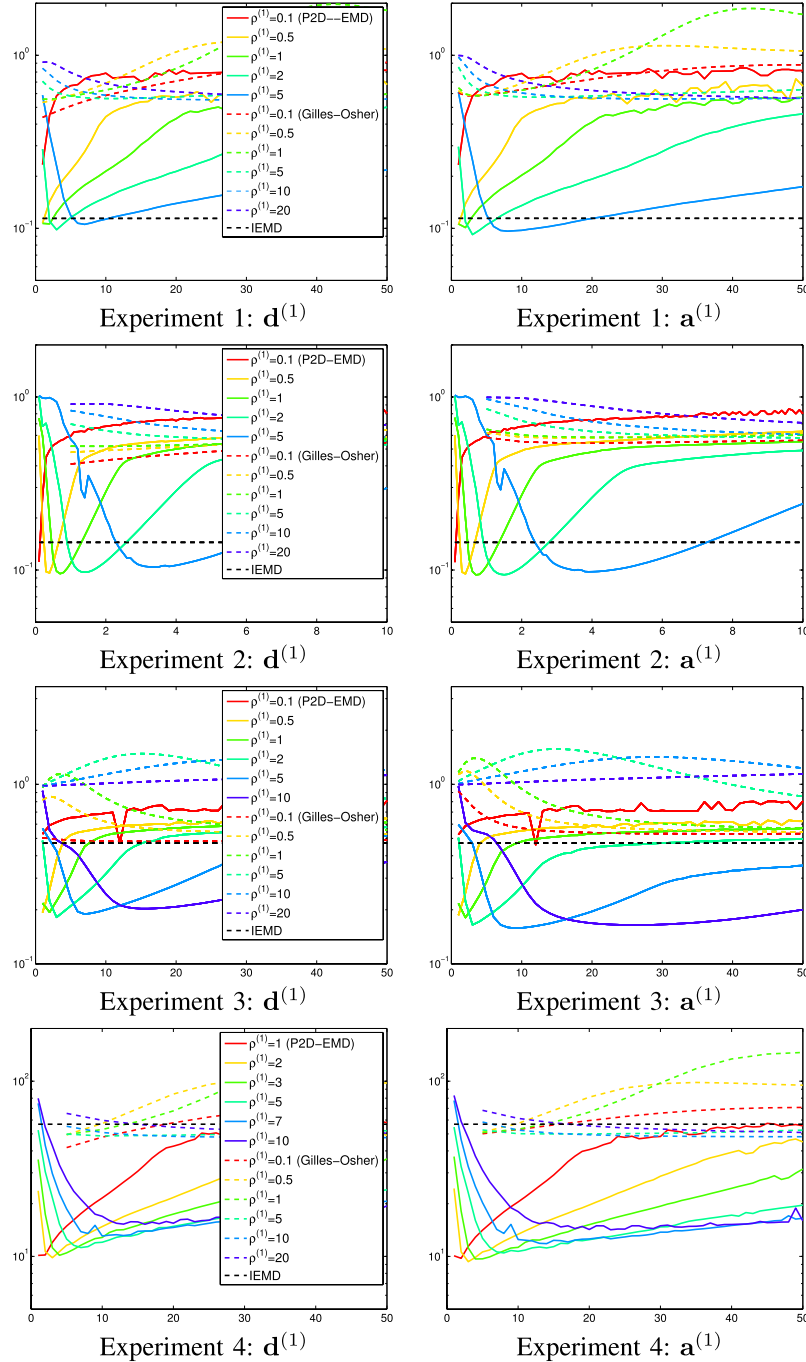


Fig. 8. Comparison of results of IEMD, Gilles-Osher and P2D-EMD on image 1. Mean square error on $\mathbf{d}^{(1)}$ (left) and $\mathbf{a}^{(1)}$ (right) with respect to the theoretical component as a function of $v^{(1)}$ for different values of $\rho^{(1)}$ for the three methods: P2D-EMD (solid lines), Gilles-Osher (color dashed line), and IEMD (black dashed line).

$$f_{m1} = 4/128, \theta_1 = \pi/3, f_{c2} = 64/128, f_{m2} = 8/128, \\ \theta_2 = \pi/4, f_{c3} = 8/128, f_{m3} = 1/128, \theta_3 = \pi/4.$$

- Experiment 4 combines the first experiment with an ellipsoidal patch: every pixel outside the ellipsoidal patch is set to zero.

The synthetic images are displayed in Fig. 9.

We provide two types of quantitative evaluation: the robustness to the parameters $v^{(1)}$ and $\rho^{(1)}$ in the decomposition step and the performance of the proposed P2D-PHT compared to P2D-HHT. Note that P2D-EMD leads to similar

performance than G2D-EMD but is much more faster. For this reason, we have limited the evaluation of the performance on P2D.

For each experiment, we evaluate the performance of the proposed P2D-EMD method with respect to the parameters $v^{(1)}$ and $\rho^{(1)}$ in terms of mean square error on the estimated $d^{(1)}$ and $a^{(1)}$ with respect to the theoretical components. We compare them with two state-of-art methods: image empirical mode decomposition [14] and a texture-geometry decomposition [24]. The results are displayed in Fig. 8. We

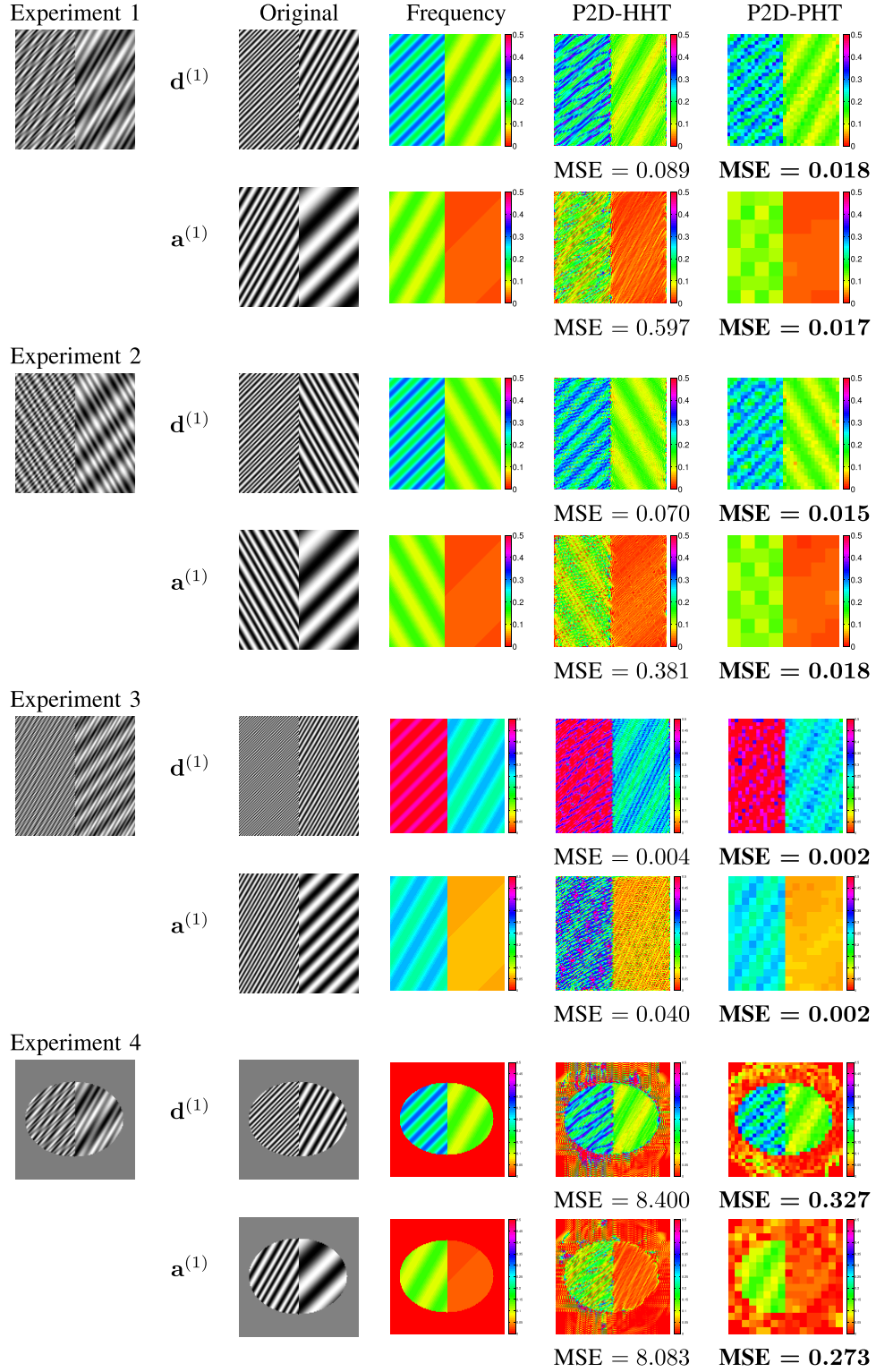


Fig. 9. Comparison of the performance in terms of frequency estimation between a monogenic analysis and the proposed Prony estimation procedure.

can observe that the proposed P2D-EMD leads to better performance for a large range of parameters $\nu^{(1)}$ and $\rho^{(1)}$. P2D-EMD clearly outperforms quantitatively the state-of-art methods. IEMD fails especially when the frequencies are high like on Experiment 3 and when the data contains piecewise continuous parts like the outside of the ellipse on

Experiment 4. Gilles-Osher method fails on the four images due to its lack of adaptivity, it is not suited for extracting oscillations of non stationary frequency.

In Fig. 9, we display the performance in terms of frequency estimation for an estimation based on a monogenic analysis and on the proposed Prony patch-based estimation.

The MSE between the real frequencies and the estimated ones is computed. We can observe that for all the experiments the Prony patch-based procedure leads to improve performance. We do not present the amplitude and orientation estimation performance because both solutions are very close except for the Experiment 4 for which the proposed method performs better.

V. CONCLUSION

This paper presents a complete method for spectral analysis of nonstationary images. This method is based on a 2D variational mode decomposition combined with a local spectral analysis method based on Prony annihilation property of cosine functions. This method has been tested on simulated and real data. For the decomposition step, our variational 2D–EMD proved to be more adaptive than other decomposition approaches like Riesz–Laplace wavelets and texture–geometry methods, and more efficient than existing 2D–EMD methods in addition of having more robustness and stronger convergence guarantees. Regarding the spectral analysis step, Prony’s annihilation-based method proved to be more efficient for frequency estimation and more robust with respect to noise and decomposition errors than monogenic analysis. The main drawback of the method is the loss of resolution due to its patch based approach. Further works should improve the resolution by introducing patch overlapping.

ACKNOWLEDGEMENTS

The authors would like to thank the two reviewers for their constructive comments that significantly helped to improve the paper.

REFERENCES

- [1] V. Ojansivu and J. Heikkilä, “Blur insensitive texture classification using local phase quantization,” in *Image and Signal Processing*, A. Elmotaz, O. Lezoray, F. Nouboud, and D. Mammass, Eds. Berlin, Germany: Springer-Verlag, 2008, pp. 236–243.
- [2] Z. Guo, L. Zhang, and D. Zhang, “Rotation invariant texture classification using LBP variance (LBPV) with global matching,” *Pattern Recognit.*, vol. 43, no. 3, pp. 706–719, Mar. 2010.
- [3] C. H. Park and H. Park, “Fingerprint classification using fast Fourier transform and nonlinear discriminant analysis,” *Pattern Recognit.*, vol. 38, no. 4, pp. 495–503, 2005.
- [4] S. Yoon, J. Feng, and A. K. Jain, “Altered fingerprints: Analysis and detection,” *IEEE Trans. Pattern Anal. Mach. Intell.*, vol. 34, no. 3, pp. 451–464, Mar. 2012.
- [5] I. Polo, A. Lazar, B. Rodriguez-Fonseca, and S. Arnault, “Oceanic Kelvin waves and tropical Atlantic intraseasonal variability: 1. Kelvin wave characterization,” *J. Geophys. Res., Oceans*, vol. 113, no. C7, Jul. 2008.
- [6] B. Alnajjar and R. S. Blum, “Ocean wave prediction for noisy sensor measurements,” in *Proc. Marine Energy Technol. Symp.*, 2013.
- [7] N. E. Huang *et al.*, “The empirical mode decomposition and the Hilbert spectrum for nonlinear and non-stationary time series analysis,” *Proc. Roy. Soc. A Math. Phys. Eng. Sci.*, vol. 454, no. 2074, pp. 903–995, Oct. 1998.
- [8] G. Jager, R. Koch, A. Kunoth, and R. Pabel, “Fast empirical mode decompositions of multivariate data based on adaptive spline-wavelets and a generalization of the Hilbert–Huang-transform (HHT) to arbitrary space dimensions,” *Adv. Adapt. Data Anal.*, vol. 2, no. 3, pp. 337–358, Jul. 2010.
- [9] Q. Chen, N. Huang, S. Riemschneider, and Y. Xi, “A B-spline approach for empirical mode decompositions,” *Adv. Comput. Math.*, vol. 24, nos. 1–4, pp. 171–195, 2010.
- [10] M. Felsberg and G. Sommer, “The multidimensional isotropic generalization of quadrature filters in geometric algebra,” in *Proc. Int. Workshop Algebraic Frames Perception-Action Cycle*, 2000, pp. 175–185.
- [11] M. Felsberg and G. Sommer, “The monogenic scale-space: A unifying approach to phase-based image processing in scale-space,” *J. Math. Imag. Vis.*, vol. 21, nos. 1–2, pp. 5–26, Jul. 2004.
- [12] M. Unser, D. Sage, and D. Van De Ville, “Multiresolution monogenic signal analysis using the Riesz–Laplace wavelet transform,” *IEEE Trans. Image Process.*, vol. 18, no. 11, pp. 2402–2418, Nov. 2009.
- [13] Z. Wu, N. E. Huang, and X. Chan, “The multi-dimensional ensemble empirical mode decomposition method,” *Adv. Adapt. Data Anal.*, vol. 1, no. 2, pp. 339–372, 2009.
- [14] A. Linderhed, “Image empirical mode decomposition: A new tool for image processing,” *Adv. Adapt. Data Anal.*, vol. 1, no. 2, pp. 265–294, Apr. 2009.
- [15] J. C. Nunes, Y. Bouaoune, E. Delechelle, O. Niang, and P. Bunel, “Image analysis by bidimensional empirical mode decomposition,” *Image Vis. Comput.*, vol. 21, no. 12, pp. 1019–1026, Nov. 2003.
- [16] C. Damerval, S. Meignan, and V. Perrier, “A fast algorithm for bidimensional EMD,” *IEEE Signal Process. Lett.*, vol. 12, no. 10, pp. 701–705, Oct. 2005.
- [17] Y. Xu, B. Liu, J. Liu, and S. Riemschneider, “Two-dimensional empirical mode decomposition by finite elements,” *Proc. Roy. Soc. A, Math., Phys. Eng. Sci.*, vol. 462, no. 2074, pp. 3081–3096, Oct. 2006.
- [18] B. Huang and A. Kunoth, “An optimization based empirical mode decomposition scheme,” *J. Comput. Appl. Math.*, vol. 240, pp. 174–183, Mar. 2012.
- [19] M.-S. Koh and E. Rodriguez-Marek, “Perfect reconstructable decimated two-dimensional empirical mode decomposition filter banks,” in *Proc. IEEE Int. Conf. Acoust., Speech Signal Process.*, May 2013, pp. 1952–1956.
- [20] T. Oberlin, S. Meignan, and V. Perrier, “An alternative formulation for the empirical mode decomposition,” *IEEE Trans. Signal Process.*, vol. 60, no. 5, pp. 2236–2246, May 2012.
- [21] T. Y. Hou, M. P. Yan, and Z. Wu, “A variant of the EMD method for multi-scale data,” *Adv. Adapt. Data Anal.*, vol. 1, no. 4, pp. 483–516, Oct. 2009.
- [22] N. Pustelnik, P. Borgnat, and P. Flandrin, “Empirical mode decomposition revisited by multicomponent non-smooth convex optimization,” *Signal Process.*, vol. 102, pp. 313–331, Sep. 2014.
- [23] J.-F. Aujol, G. Gilboa, T. Chan, and S. Osher, “Structure-texture image decomposition—Modeling, algorithms, and parameter selection,” *Int. J. Comput. Vis.*, vol. 67, no. 1, pp. 111–136, Apr. 2006.
- [24] J. Gilles and S. Osher, “Bregman implementation of Meyer’s G-norm for cartoon+textures decomposition,” Dept. UCLA Comput. Appl. Math. Rep., UCLA, Los Angeles, CA, USA, Tech. Rep. CAM11-73, Nov. 2011.
- [25] J. Gilles, “Multiscale texture separation,” *Multiscale Model. Simul.*, vol. 10, no. 4, pp. 1409–1427, Dec. 2012.
- [26] S. M. Kay and S. L. Marple, Jr., “Spectrum analysis—A modern perspective,” *Proc. IEEE*, vol. 69, no. 11, pp. 1380–1419, Nov. 1981.
- [27] G. M. Riche de Prony, “Essai expŽimental et analytique : Sur les lois de la dilatabilitŽ de fluides Žlastiques et sur celles de la force expansive de la vapeur de l’eau et de la vapeur de l’alcool diffŽrentes tempŽratures,” *J. Ecole Polytechn.*, vol. 1, no. 22, pp. 24–35, 1795.
- [28] S. Stoica and R. L. Moses, *Introduction to Spectral Analysis*. Englewood Cliffs, NJ, USA: Prentice-Hall, 1988.
- [29] S. M. Kay, *Modern Spectral Estimation Theory and Application*. Englewood Cliffs, NJ, USA: Prentice-Hall, 1988.
- [30] T. Blu, P.-L. Dragotti, M. Vetterli, P. Marziliani, and L. Coulot, “Sparse sampling of signal innovations,” *IEEE Signal Process. Mag.*, vol. 25, no. 2, pp. 31–40, Mar. 2008.
- [31] J. A. Cadzow, “Signal enhancement—A composite property mapping algorithm,” *IEEE Trans. Acoust., Speech, Signal Process.*, vol. 36, no. 1, pp. 49–62, Jan. 1988.
- [32] L. Condat and A. Hirabayashi, “Cadzow denoising upgraded: A new projection method for the recovery of dirac pulses from noisy linear measurements,” to be published.
- [33] L. Condat, J. Boulanger, N. Pustelnik, S. Sahnoun, and L. Sengmanivong, “A 2-D spectral analysis method to estimate the modulation parameters in structured illumination microscopy,” in *Proc. IEEE 11th Int. Symp. Biomed. Imag. (ISBI)*, Apr./May 2014, pp. 604–607.

- [34] Z. Liu and S. Peng, "Boundary processing of bidimensional EMD using texture synthesis," *IEEE Signal Process. Lett.*, vol. 12, no. 1, pp. 33–36, Jan. 2005.
- [35] Y. Meyer, *Oscillating Patterns in Image Processing and Nonlinear Evolution Equations: The Fifteenth Dean Jacqueline B. Lewis Memorial Lectures*. Boston, MA, USA: AMS, Mar. 2001.
- [36] F. Luisier and T. Blu, "SURE-LET multichannel image denoising: Inter-scale orthonormal wavelet thresholding," *IEEE Trans. Image Process.*, vol. 17, no. 4, pp. 482–492, Apr. 2008.
- [37] S. Ramani, T. Blu, and M. Unser, "Monte-Carlo sure: A black-box optimization of regularization parameters for general denoising algorithms," *IEEE Trans. Image Process.*, vol. 17, no. 9, pp. 1540–1554, Sep. 2008.
- [38] J.-C. Pesquet, A. Benazzza-Benyahia, and C. Chaux, "A SURE approach for digital signal/image deconvolution problems," *IEEE Trans. Signal Process.*, vol. 57, no. 12, pp. 4616–4632, Dec. 2009.
- [39] C.-A. Deledalle, S. Vaiter, G. Peyré, J. Fadili, and C. Dossal, "Unbiased risk estimation for sparse analysis regularization," in *Proc. 19th IEEE Int. Conf. Image Process.*, Orlando, FL, USA, Sep./Oct. 2012, pp. 3053–3056.
- [40] L. Condat, "A primal-dual splitting method for convex optimization involving Lipschitzian, proximable and linear composite terms," *J. Optim. Theory Appl.*, vol. 158, no. 2, pp. 460–479, 2013.
- [41] P. L. Combettes and J.-C. Pesquet, "Primal-dual splitting algorithm for solving inclusions with mixtures of composite, Lipschitzian, and parallel-sum type monotone operators," *Set-Valued Variat. Anal.*, vol. 20, no. 2, pp. 307–330, Jun. 2012.
- [42] L. M. Briceño-Arias, P. L. Combettes, J.-C. Pesquet, and N. Pustelnik, "Proximal algorithms for multicomponent image recovery problems," *J. Math. Imag. Vis.*, vol. 41, nos. 1–2, pp. 3–22, Sep. 2011.
- [43] B. C. Vũ, "A variable metric extension of the forward-backward-forward algorithm for monotone operators," *Numer. Funct. Anal. Optim.*, vol. 34, no. 9, pp. 1050–1065, Jul. 2013.
- [44] P. L. Combettes and J.-C. Pesquet, "Proximal splitting methods in signal processing," in *Fixed-Point Algorithms for Inverse Problems in Science and Engineering*, H. H. Bauschke, R. Burachik, P. L. Combettes, V. Elser, D. R. Luke, and H. Wolkowicz, Eds. New York, NY, USA: Springer-Verlag, 2010, pp. 185–212.
- [45] T. Blu, "The generalized annihilation property—A tool for solving finite rate of innovation problems," in *Proc. Int. Workshop Sampling Theory Appl. (SampTA)*, Marseille, France, May 2009.
- [46] P. Stoica and A. Nehorai, "MUSIC, maximum likelihood, and Cramer-Rao bound," *IEEE Trans. Acoust., Speech, Signal Process.*, vol. 37, no. 5, pp. 720–741, May 1989.
- [47] R. Roy and T. Kailath, "ESPRIT-estimation of signal parameters via rotational invariance techniques," *IEEE Trans. Acoust., Speech, Signal Process.*, vol. 37, no. 7, pp. 984–995, Jul. 1989.
- [48] P. Stoica and K. C. Sharman, "Novel eigenanalysis method for direction estimation," *IEE Proc. F, Radar and Signal Process.*, vol. 137, no. 1, pp. 19–26, Feb. 1990.
- [49] P. Stoica and K. C. Sharman, "Maximum likelihood methods for direction-of-arrival estimation," *IEEE Trans. Acoust., Speech, Signal Process.*, vol. 38, no. 7, pp. 1132–1143, Jul. 1990.
- [50] M. Viberg, B. Ottersen, and T. Kailath, "Detection and estimation in sensor arrays using weighted subspace fitting," *IEEE Trans. Signal Process.*, vol. 39, no. 11, pp. 2436–2449, Nov. 1991.
- [51] J. Schmitt, N. Pustelnik, P. Borgnat, and P. Flandrin, "2D Hilbert–Huang transform," in *Proc. Int. Conf. Acoust., Speech Signal Process.*, 2013.



Jérémie Schmitt received the Ph.D. degree in signal and image processing from the Université Paris-Sud, Orsay, France, in 2011. From 2011 to 2012, he was a Post-Doctoral Research Associate with the Laboratoire de Signaux et Systèmes de l'École Supélec, Paris, France. Since 2012, he has been a Post-Doctoral Research Associate with the Signal Processing Team, Laboratoire de Physique, École Normale Supérieure de Lyon, Lyon, France. His area of interest includes mode decomposition, inverse problems, and image restoration.



Nelly Pustelnik received the Ph.D. degree in signal and image processing from the Université Paris-Est, Marne-la-Vallée, France, in 2010. From 2010 to 2011, she was a Post-Doctoral Research Associate with the Laboratoire IMS, Université de Bordeaux, Bordeaux, France, working on the topic of tomographic reconstruction from a limited number of projections. Since 2012, she has been a CNRS Researcher with the Signal Processing Team, Laboratoire de Physique de l'ENS de Lyon. Her activity is focused on inverse problems, nonsmooth convex optimization, mode decomposition, and texture analysis.



Pierre Borgnat has been a Researcher in Signal Processing with the Laboratoire de Physique, ENS de Lyon, CNRS, France, since 2004. Born in 1974, he entered ENS de Lyon in 1994, got Aggregation in physical sciences in 1997, Ph.D. degree in physics and signal processing in 2002. He worked at IRS, IST, Lisbon, Portugal, in 2003. His research interests are in statistical signal processing of nonstationary processes, scaling phenomena, and in processing of graph signals and complex networks. He works on many applications in networking, Internet traffic modeling, measurements, and classification for physics, social, or transport data analyses.



Patrick Flandrin (M'85–SM'01–F'02) received the Engineering degree from ICPI Lyon, France, in 1978, and the Dr.Ing. and Docteur d'État degrees from INP Grenoble, France, in 1982 and 1987, respectively. He joined CNRS in 1982, where he is currently the Research Director. Since 1991, he has been with the Signals, Systems and Physics Group, Department of Physics, ENS de Lyon, France. He is currently the President of GRETSI, the French Association for Signal and Image Processing. His research interests include mainly nonstationary signal processing (with an emphasis on time-frequency and time-scale methods), self-similar stochastic processes, and complex systems. He published many research papers and authored one monograph in those areas. Past Associate Editor of the *IEEE TRANSACTIONS ON SIGNAL PROCESSING* (1993–1996 and 2008–2011) and former member of the Signal Processing Theory and Methods Technical Committee of the IEEE Signal Processing Society (1993–2004), he is currently on the Editorial Board of the *IEEE Signal Processing Magazine*.

Dr. Flandrin was awarded the Philip Morris Scientific Prize in Mathematics (1991), the SPIE Wavelet Pioneer Award (2001), the Prix Michel Monpetit from the French Academy of Sciences (2001), and the Silver Medal from CNRS (2010). He has been a fellow of EURASIP (2009) and a member of the French Academy of sciences (2010).



Laurent Condat received the Ph.D. degree in applied mathematics from the Grenoble Institute of Technology, Grenoble, France, in 2006. From 2006 to 2008, he was a Post-Doctoral Researcher with Helmholtz Zentrum München, Munich, Germany. Since 2008, he has been a permanent Research Fellow with CNRS. From 2008 to 2012, he was with GREYC, Caen, France, and since 2012, he has been with the Department of Images and Signals, GIPSA-Lab, University of Grenoble-Alpes, Grenoble. His area of interest includes optimization, sampling, and inverse problems in signal and image processing.

Dr. Condat received the Best Student Paper Award at the conference IEEE ICIP in 2005 and a Best Ph.D. Award from the Grenoble Institute of Technology in 2007.